Experimental Setup for Rydberg Spectroscopy

von

Igor Marinković

Masterarbeit in Physik

angefertigt im
Institut für Angewandte Physik

vorgelegt der
Mathematisch-Naturwissenschaftlichen Fakultät
der Rheinischen Friedrich-Wilhelms-Universität Bonn

Oktober 2014

Referent: Prof. Dr. D. Meschede
Koreferent: Prof. Dr. M. Weitz

Abstract

This master thesis describes a setup for optically exciting Rubiduim 87 atoms to Rydberg states. A two photon scheme is implemented to transfer atoms from the ground state to the Rydberg state, using laser light at 780 nm and 480 nm. In order to achieve the required short and long term stability, the diode laser at 780 nm is locked to an Ultra Low Expansion (ULE) glass cavity, which is placed inside vacuum, vibrationally isolated and thermally stabilized. Laser light at 480 nm is produced by frequency doubling light from a 960 nm laser, using a BIBO crystal inside an enhancement cavity.

We have demonstrated the systems ability to address Rydberg states in ^{87}Rb, by performing Electromagnetically Induced Transparency (EIT) spectroscopy in a room temperature vapor cell. In the future EIT can be used for the locking of the 480 nm laser via frequency modulation spectroscopy.

Contents

Abbreviations

VCO	voltage controlled oscillator
AOM	acousto-optic modulator
VCA	coltage controlled attenuator
EOM	electro-optic modulator
RF	radio-frequency
PBS	polarizing beam splitter
PD	photodiode
m_e	mass of electron
Ry	Rydberg constant
$\hbar$	Planck constant
e	electron charge
k_b	Boltzmann constant
ϵ_0	dielectric constant
c	speed of light

Introduction

Starting with Feynman's famous idea in 1982 [1], a huge amount of theoretical work has been done in order to explore the possibilities of computation using objects behaving by the rules of quantum mechanics [2, 3]. This work showed that one can expect that such a device will be able to perform certain tasks much faster than computers nowadays. From this, Quantum Information (QI) science was born, but only in theory. The task of implementing a quantum computer, which can outperform classical computers, still remains. Besides practical interests, building a quantum devices allows to address fundamental questions if nature indeed behaves quantum mechanically.

Several fields of physics have contributed to the goal of realizing a quantum computer for years now. Therefore the physical systems that are considered as potential qubits are diverse: ions [4], neutral atoms [5], superconductors [6], quantum dots [7]... and combinations of these systems. In several of these systems the basic ingredients for quantum computation [8] have been demonstrated. Each of these physical implementations has its benefits and disadvantages. This thesis is concerned with neutral atoms, for which scalability represents one of the largest challenges.

Neutral atoms started being potential candidate for QI processing after the development of techniques for their trapping and cooling. Single particles can be isolated from the classical world and their states controlled while preserving their quantum properties. This makes the well defined atomic systems excellent qubits. But, because of a weak interaction, it is hard to produce entanglement between neutral atoms, which is a key ingredient for QI processing. There are proposals how to entangle neutral atoms besides using Rydberg states [5, 9, 10]. The speed of entanglement in these proposals is limited by the weak interaction of the atoms in ground states. In this and next chapter we will motivate why Rydberg atoms are considered as a system that might help overcoming this problem.

A Rydberg atom is an atom whose electron is excited to a state with a high value of principal quantum number n. An important feature of Rydberg states is their strong interaction (due to large electron-core distance) and that can be tuned over an enormous range. Neutral atoms in the ground state interact weakly, but by exciting them to Rydberg states one can enhance the interaction between them by more than 10 orders of magnitude [11]. Strength of interaction depends has a strong dependence on the specific Rydberg state which has been excited.

Generally for the QI processing following statement holds. *"Strong interactions are required*

to implement fast quantum gates, and long-term storage is achieved in the non-interacting regime" [12]. In Rydberg atoms this switching between interacting and non-interacting regime is done simply by excitation and de-excitation. The idea to use cold Rydberg atoms for realising quantum gates started in 1999 [13]. Here, it was for the first time pointed out that a strong tunable state dependant interaction makes the Rydberg atoms a valuable tool for QI processing using neutral atoms.

Experimentally the first Rabi oscillations between ground and Rydberg state were observed in 2006 [14]. Soon after, C-NOT gates between two neutral atoms based on Rydberg interaction were performed [15], that used two hyperfine ground states of atoms as qubit states.

Since then several other approaches how to use Rydberg atoms for QI tasks have been developed. Strong interactions of Rydberg atoms have also been used to realize photonic quantum gates [16]. Here information is encoded in states of photons instead of the atoms, and the atoms are used to induce "interaction" between the photons, who otherwise do not interact.

Also, Rydberg excitations can form the basis for atom-photon interfaces. Deterministic entanglement of ensemble of atoms and photon using Rydberg atoms has been demonstrated [17]. This is a key ingredient for a quantum network, where nods of network are atoms and information is transmitted using photons.

The research of Rydberg atoms in this group will go in the direction of producing and investigating Rydberg atoms inside a high-finesse cavity. This should lead to very strong coupling between light and atoms, since both the cavity enhanced interaction and the Rydberg non-linearity will play role. There have been some theoretical considerations [18], that suggest that interesting effects like an enhanced blockade radius can be expected. Cooling and trapping techniques for neutral atoms have already been implemented in FCQED lab and Rydberg setup is planned to be add-on that will give the setup additional features (entanglement, single photon sources).

Structure of this thesis is following. In Chapter 1, Rydberg atoms and their properties will be discussed. This should give an idea what requirements the setup needs to fulfil in order to perform experiments with Rydberg atoms and utilize their properties for QI processing. The following chapters will explain in more detail individual parts of the setup. Each chapter will start with brief theoretical background, then the setup will be presented, and finally results of characterization of each part will be shown.

Rydberg atoms

Here the properties of Rydberg atoms will be described in more detail. Most important in this discussion is the interaction between Rydberg stoms and the effect of the Rydberg blockade that arises from it. At the end of this chapter, an overview of setup for Rydberg experiments, which has been built during this thesis, will be presented.

2.1 Properties of Rydberg atoms

The internal energy level structure of Rydberg atoms of alkalis is very similar to the structure of the hydrogen atom, because of the presence of only one valence electron, which is shielded from nucleus by other electrons. The simple equation

$$E_r = -\frac{Ry}{(1 + m_e/m_n)(n - \delta(l))^2} = -\frac{Ry}{(1 + m_e/m_n)(n^*)^2} \tag{2.1.1}$$

gives the electronic energy levels of Rydberg states [19], where m_n is mass of nucleus and $\delta(l)$ is phenomenological constant called quantum defect, that has to be included since shielding is not perfect.

However, due to large electron-nucleus separation in high lying Rydberg states, these atoms exhibit some extreme atomic properties. The scaling of some of them with effective principle quantum number (n^*) is given in Table 2.1. At short distances between Rydberg atoms strong dipole-dipole interaction is dominant. At long distances interaction between Rydberg atoms is van der Waals type, that scales $V(R) = C_v/R^6$.

Property	Scaling	Rb(5s)-ground	Rb(43s)-Rydberg
Orbit radius	$(n^*)^2$	$5.632 \cdot a_0$	$2384.2 \cdot a_0$
Polarizability	$(n^*)^7$	-79 mHz(Vcm^{-1})$^{-2}$	-18 MHz(Vcm^{-1})$^{-2}$
Lifetime	$(n^*)^3$	$5p_{3/2} \rightarrow 5s_{1/2}$: 26.2 ns	42.3 µs
van der Waals coef. C_v	$(n^*)^2$	4707 au	-1.69$\cdot 10^{19}$ au

Table 2.1: Scaling of some important Rydberg atom properties (values taken from [19]) and as an example comparison of values between ground and $43s$ state of ^{87}Rb. a_0 is Bohr radius.

2.2 Rydberg blockade

Now let us consider an ensemble of atoms that are being illuminated with light that is resonant with a single atom Rydberg transition. If a single atom in the ensemble was excited to the Rydberg state, then the energy levels of all other atoms would be shifted out of resonance with respect to the exciting laser (assuming the laser linewidth is narrow enough), due to strong Rydberg interaction between atoms. So, as soon as one atom is excited to Rydberg state then other atoms can not be excited. Moreover if, all atoms in the ensemble are identical, the one excitation that exists will be shared between all of them. This collective state will be common for all atoms within the sphere of radius $R_b = (C_v/\hbar\Omega_r)^{1/6}$ [20]. Here C_v is the van der Waals coefficient and Ω_r is the Rabi frequency between the ground (g) and Rydberg (r) states. This phenomena is known as a Rydberg blockade and R_b is Rydberg blockade radius. A state created in this fashion can be written as

$$| \psi >= \frac{1}{\sqrt{N}} \sum_{i=1}^{N} | g_1 g_2 ... r_i ... g_N >,$$

where N is the number of atoms in the ensemble. The whole sphere acts as a single two level atom, where the Rabi frequency is enhanced by $\sqrt{N}$ compared to the single atom Rabi frequency. This ensemble is extremely non-linear since it can absorb only one photon. Also, one notices that the cross section is N times bigger than for single atom. Such an ensemble is often called superatom. It is can be looked at as a nonlinear oscillator with large cross section. The enhancement of the Rabi frequency has been demonstrated in several papers [21]. Furthermore, a single photon source based on Rydberg blockade has been implemented in [12]. This is done by first exciting small ensemble such that there is only one Rydberg excitation, because of blockade. Subsequent de-excitation pulse will produce a single photon.

The blockade effect is an essential part of quantum gate proposal and implementation mentioned in previous section. The basic idea is that one atom can, by blockade, control the transitions and therefore the state of the other atom. Because of long range interaction, atoms can be placed few micrometers away and individually addressed with optical fields.

In most experiments, cold atoms in electronic ground state are first trapped using optical lattice. Then the trapping field is switched off because it is actually repulsive for Rydberg atoms. After that Rydberg excitations can be done for short time, before atoms diffuse away. Recently, trapping of atoms in Rydberg states has been realized [22]. This is a significant step forward and might enable higher efficiency of quantum gates.

Rydberg atoms are not only being used in the cold atom experiments. Rabi oscillationa are also observed in hot Rydberg atoms [23]. Because of the fast decoherence in such systems one needs Rabi flopping on the GHz time scale, which can be done using pulsed lasers. This decreases the effect of the Rydberg blockade, but only weakly because of the $(1/\Omega_r)^{1/6}$ dependence.

As we have motivated here, Rydberg atoms have unique properties enabling them to create
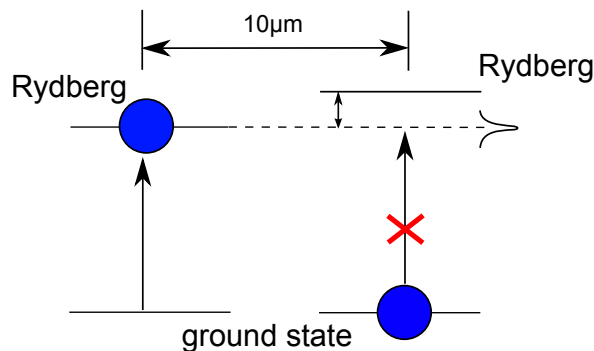
Figure 2.1: Rydberg blockade phenomena. The atom on the right can not be excited to Rydberg state because of the interaction with the atom on the left which is in the Rydberg state. The energy of Rydberg state of atom on the right is shifted relative to the situation with no interaction (dashed).

strong optical non-linearities, and making them an interesting topic in the field of quantum optics and quantum information.
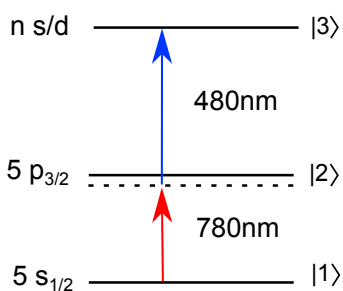
2.3   Setup overview

Figure 2.2: Excitation scheme. Rydberg states are produced with two lasers with wavelengths of 780 nm and 480 nm. The detuning from an intermediate level is present in order to avoid spontaneous emission.

In this thesis, Rydberg states of Rubidium 87 atoms are considered. Single photon excitation to the Rydberg states is possible using 297 nm light, but this method is sensitive to Doppler shifts and working with ultraviolet light is always a technical challenge. Therefore, a two photon excitation scheme (Figure 2.2) using 780 nm and 480 nm light is chosen for this experiment. This way the Rydberg s and d states can be addressed.

In order to excite atoms and produce the effect of the Rydberg blockade, the excitation lasers have to exhibit a linewidth and long term stability, which is smaller than interaction shift. In practice the laser linewidth should be the order of few tens of kHz (for usual quantum information experiments). In addition transition matrix element to Rydberg states are very small. For coherent excitation it is necessary that Rabi frequency is much larger than linewidth
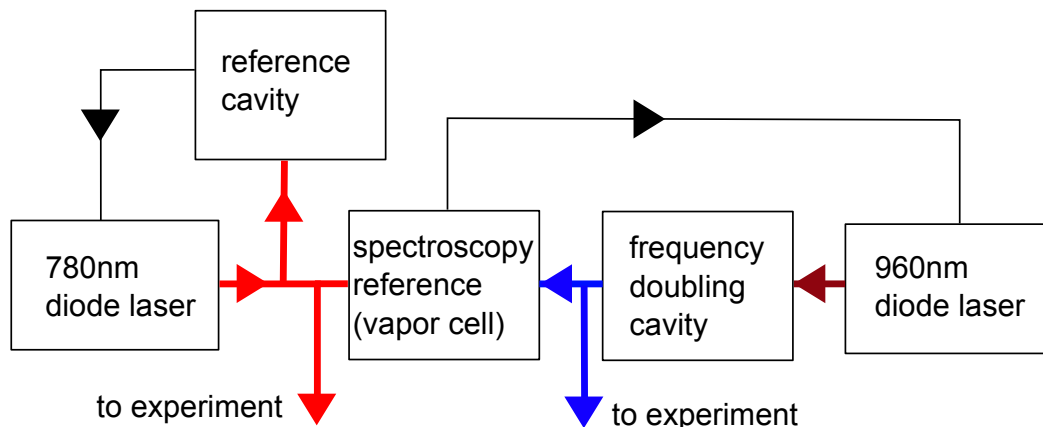
Figure 2.3: Schematic overview. The setup generates light at 780 nm and 480 nm and provides the frequency references for each of them.

of Rydberg transition (tens of kHz). Now, we would like to estimate power of the light at 480 nm (blue) needed to produce Rabi frequency on MHz scale. At distance of around few µm the shift due to Rydberg interaction is also around MHz, so we assume that excitation lasers are focused to 10 µm. Rabi frequency of 780 nm excitation is $2\pi \cdot 100$ MHz and single photon detuning is 1 GHz (needed to reduce spontaneous emission from intermediate state). In order to achieve two photon Rabi frequencies on MHz scale for high lying states, it is necessary that the power of the blue laser should be on the order of 100 mW.

Building up a laser system with these characteristics is the main goal of this thesis. A schematic overview of experimental setup is given in Figure 2.3. Light at 780 nm (red) is produced using diode laser and it is locked to reference cavity. Locking is the process of comparing laser's frequency to stable reference and correcting it such that it always matches to reference. That way narrow linewidth and long term stability are obtained. Light at 480 nm (blue) is produced by frequency doubling light from a laser diode at 960 nm. In this case Rydberg electromagnetically induced transparency (EIT) in the vapor cell will be used as a frequency reference. How to set up a stable reference cavity and characterize it, is topic of Chapter 3. Locking the laser relative to the cavity will be presented is Chapter 4. The following chapter will show the setup for producing 480 nm light by frequency doubling. Finally coupling to the Rydberg states will be demonstrated using EIT in Chapter 6.

Reference cavity

For exciting Rubidium atoms to intermediate state, laser light at 780 nm is needed which is stabilized by some external reference. As a reference, an atom transition or a cavity are often used. Atomic transitions are exploited for locking usually by preforming one of several Doppler free spectroscopy techniques [24] in vapor cells. In this setup a reference cavity will be used. This chapter is describing a process of building, optimizing and characterising a passively stable frequency reference for the red laser.

3.1 Optical cavity

Light at 780 nm is produced by a home built interference filter laser (for details of the design see [25]). The frequency of these lasers tends to drift over large range, but it is possible to externally control their frequency. In order to have a fixed laser frequency, a stable reference is needed, to which the frequency can be compared and corrected.
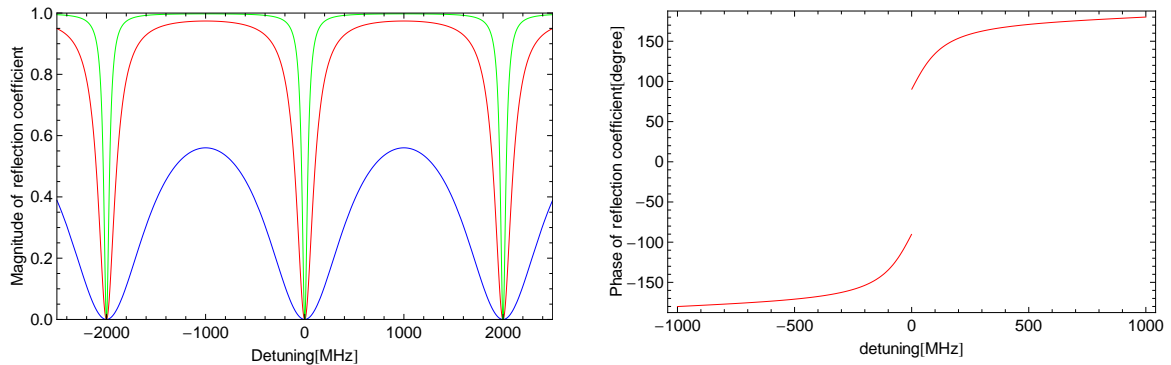

Figure 3.1: Left: Magnitude of reflection coefficient of a cavity with length of 1, and various reflection coefficients of mirrors. $r(green) = 0.95$, $r(red) = 0.85$, $r(blue) = 0.45$. The distance between dips is called the free spectral range, and it is determined by the length of the cavity. In this case $\Delta\nu_{fsr} = 2000$ MHz. Right: Phase response of cavity for $r(red) = 0.85$.

Optical cavities can transmit or reflect light depending on frequency of light. Therefore by looking at the amount of reflected light, the cavity can be used as a frequency discriminator. The derivation of reflection coefficient of optical cavities with flat mirrors can be found in many optics textbooks [26]. Here, we just give its final expression for the case of equal reflectivity of mirrors

$$F = \frac{E_r}{E_i} = r \frac{e^{i\frac{4\pi L}{c}} - 1}{1 - r^2 e^{i\frac{4\pi L}{\lambda}}}, \tag{3.1.1}$$

where E_r and E_i are reflected and incident field amplitude, r is mirror reflectivity, L length of cavity and λ is wavelength of light. The magnitude of the cavity reflection coefficient for an exemplary cavity is plotted in the left part of Figure 3.1. It describes the intensity of the reflected wave. Its phase relative to the incident wave is plotted in the right part. Dips in the intensity of the reflected wave are often referred to as cavity resonances, and their center positions are given by the standing wave condition

$$\nu = m\frac{c}{2nL}, \quad m = 1, 2, 3... \tag{3.1.2}$$

So, having a stable length and refractive index will result in a stable resonant frequency of a cavity. This can be achieved, by having the environment of the cavity controlled and stabilized. Light that is coupled into cavity makes a lot of round trips between mirrors, before it finally leaves the cavity. The linewidth of the cavity is given by the decay time that is needed for light to leak out of the cavity

$$\Delta\nu = \frac{1}{2\pi\tau}. \tag{3.1.3}$$

In general, the narrower a linewidth of the resonance, the more precise a cavity can be as a reference.

Another quantity often used to describe a cavity is its finesse (the number of round trips)

$$\mathcal{F} = \frac{\tau c \pi}{L} \tag{3.1.4}$$

The cavity used in this setup was originally designed to be used for 850 nm light [27]. It is 7.5 cm long and the free spectral range is $\Delta\nu_{fsr} = \frac{c}{2L} = 2\,\text{GHz}$. Its spacer is made out of Ultra Low Expansion (ULE) glass that has very low thermal expansion coefficient, which ensures long term stability of cavity length. The finesse of cavity for light at 850 nm is about 70000 [27]. The measurement of finesse for light at 780 nm is presented in Section 3.2.

Cavities with plain mirror are not commonly used because they are very sensitive to mirror misalignments. Our cavity mirrors have radius of curvature of $R = 1\,\text{m}$. Such a cavity has a more complicated spectrum, than the case we previously considered. A lot of resonances are present corresponding to to different transversal modes. Here we would like to couple light only to the Gaussian mode. The coupling to higher modes can be suppressed by proper mode

matching. That means that the input beam should have same path and waist as Gaussian mode of cavity. The waist of the Gaussian mode inside a symmetric cavity is given by [28]

$$w = \left(\frac{\lambda}{\pi}\right)^{1/2} \left(\frac{L}{2}\right)^{1/4} \left(R - \frac{L}{2}\right)^{1/4} \approx 220\,\mu\text{m}$$

3.2 Setup for the reference cavity

In order to keep changes of the cavity resonance frequency small, fluctuations of the length and the refractive index of the cavity needs to be minimized. The reasons for these fluctuations are usually acoustic vibrations and variations of pressure and temperature. Due to temperature changes and vibrations, the length of the spacer changes. The index of refraction changes both due to temperature and pressure changes. Therefore, as a first step, the cavity is placed inside of a vacuum chamber. Primarily this reduces pressure fluctuations that lead to fluctuations of the refractive index. Also, thermal variations and vibrations are reduced this way.
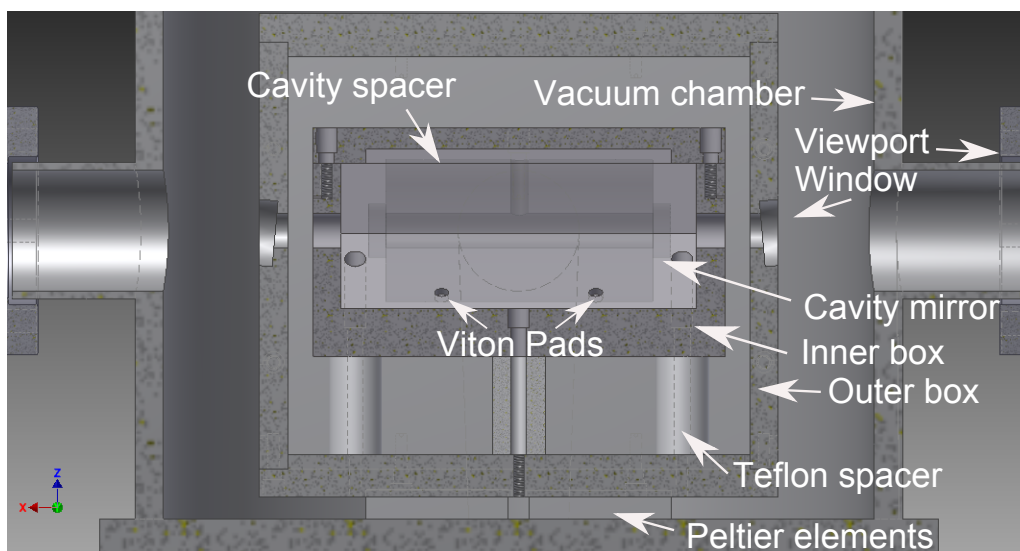

Figure 3.2: Cross section of CAD model of the vacuum chamber with aluminium boxes and cavity inside. The CAD model is made using Autodesk Inventor software.

Inside the vacuum chamber there are two thermally isolated aluminium boxes that provide good thermal stability for cavity that is inside them. These boxes are manufactured by the institute's workshop, according to CAD drawings (Figure 3.2). The cavity is placed inside the inner aluminium box, that has a V-shaped block as the bottom plate. On V-block there are four Viton pads that support the cavity. They are placed on so called Airy points (0.21L from ends) [29], which should minimize the length sensitivity to vibrations. The angle between normals on the Viton pads is 70°. The inner box is separated from the outer box by five teflon spacers that serve as a thermal isolator. Each screw hole has an additional hole from side, so

air is properly evacuated. Both boxes have bores through which the laser beam can pass. Two AR coated windows are placed on outer box to prevent thermal radiation to reach the cavity. Together with chamber windows they are tilted by 5° to avoid the etalon effect. The outer box rests on four Peltier elements (Laird Technologies MS2,192,14,20,15,25) that are used for temperature stabilization of outer box. In order to have a good thermal conductivity with the heat sink (vacuum vessel), Peltier elements are glued on both sides using Stycast glue, that has good thermal conductivity and is vacuum compatible. Temperature of outer box is monitored with NTC thermistor (EPCOS - B57560G103F). Peltier elements are also needed in order to keep cavity at a zero expansion temperature (see Section 2.4). Initially the Stycast glue was not used, and the outer box was resting just on Peltier elements. This setup was tested before evacuating the chamber and it was working. After evacuating, the system failed after few minutes. Most likely the air had been enough to take away heat from the hot side of Peltiers. Once the air was removed, Peltier elements would heat up and desolder, because of a bad heat sink. This caused the setup failure. Adding Stycast glue to improve the thermal contact, fixed this problem. The temperature control elements are electrically connected to feedthrough using Kapton wires that are vacuum compatible.

After closing the vacuum chamber turbopump is used for to reach 10^{-4}mbar, then the ion pump is started. The turbopump is then turned off and detached, because it produces a lot of mechanical noise, that would influence the stability of the cavity. The pressure inside the vacuum chamber is below 10^{-7}mbar. Before the final closing, the chamber is for the first time evacuated without the cavity inside and baked out. High temperature can potentially damage coating of the cavity mirrors.
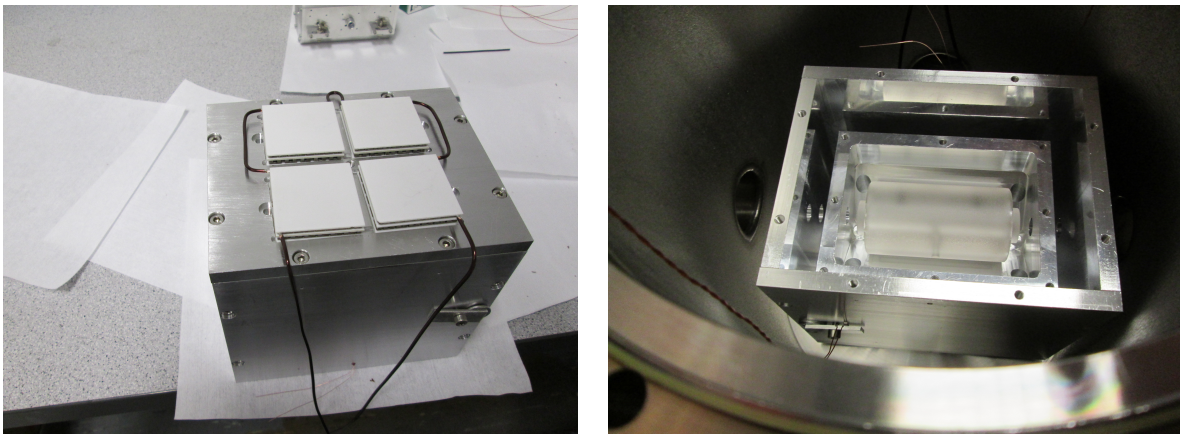

Figure 3.3: Left: Peltier elements placed on baseplate of outer aluminium box. Right: Cavity inside boxes.

The whole chamber is placed on an optical breadboard, which rests on Sorbothane pads on the optical table. This provides an additional vibration isolation. All fiber and optical elements needed for coupling light into the cavity are placed on same breadboard as the chamber (see
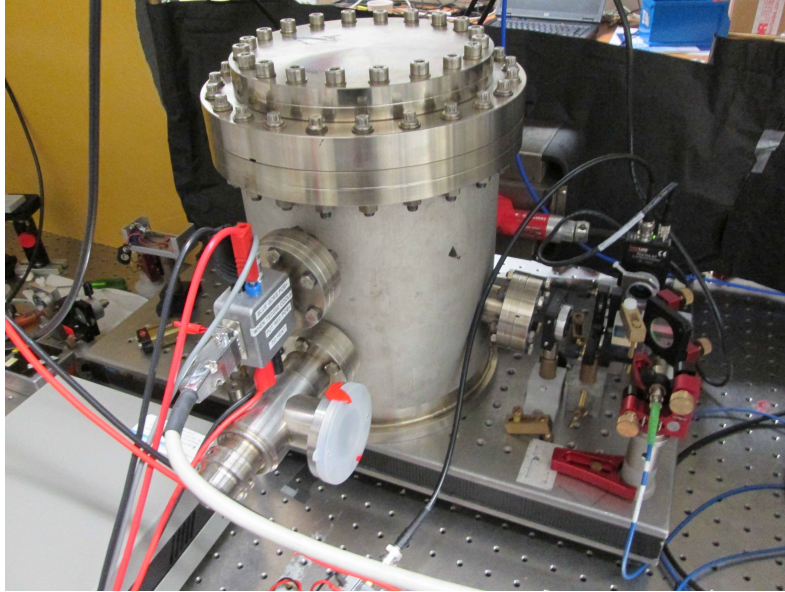
Figure 3.4: Vacuum chamber on a breadboard. The laser is placed on another breadboard and the fiber is used as an optical connection between two. On the left side, underneath the electrical feedthrough one can see the valve to which the turbopump was attached.

Figure 3.4). At one end of the fiber the light from 780 nm diode laser is coupled in, and the other end is used for coupling into the cavity. For this purpose, the waist is adjusted using the fiber collimator and putting the cavity at a right distance. An additional mirror is used, together with the fiber holder, for the beam walking so that the paths are aligned.

3.3   Ring down measurement

In order to characterize the linewidth of the cavity the ring down method is used. This method, which determines the time that is needed for light to leak out of the cavity, is practical for characterizing narrow linewidth cavities since their decay time is long. For wide linewidth cavities the decay time could be to short to detect.

The setup for ring down measurement is shown in Figure 3.5. Light from the red laser is sent through an AOM and coupled into the cavity. Here, the AOM is used as a switch. The laser is scanned over the cavity resonance. Transmitted light is detected with a photodiode (Thorlabs PDA10A), that is connected to an oscilloscope. The external trigger output of oscilloscope is connected to the RF switch that can control the RF power going into the AOM. Once light is coupled into the cavity and the signal on the photodiode rises to certain level, the AOM is switched off and a decaying curve is obtained, as in Figure 3.6. The oscilloscope is set to average the data on 32 measurements. Fitting the data with an exponential, one can determine the decay time.

There is also some delay coming from the finite switching time and response time of photodiode.
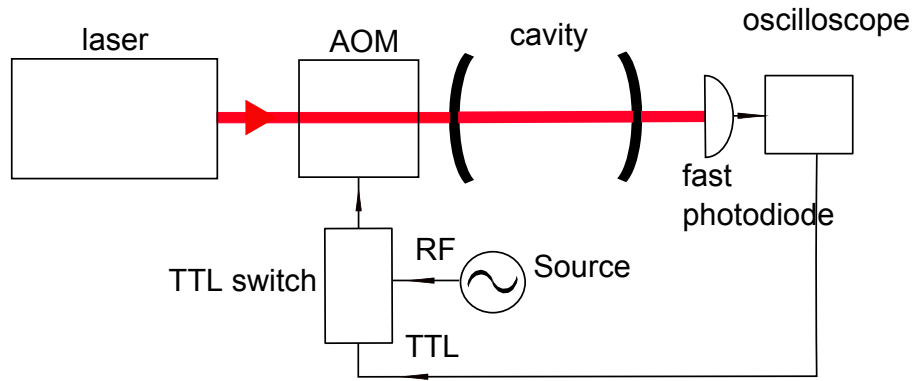
Figure 3.5: Setup for the cavity ring down measurement. Initially the AOM is turned on, such that light is sent to the cavity and the laser is being scanned. As soon as some amount of light is coupled into the cavity, oscilloscope and RF switch automatically turn off the AOM and no light is going to the cavity. This way the leaking of the light that has been coupled before switching can be observed.
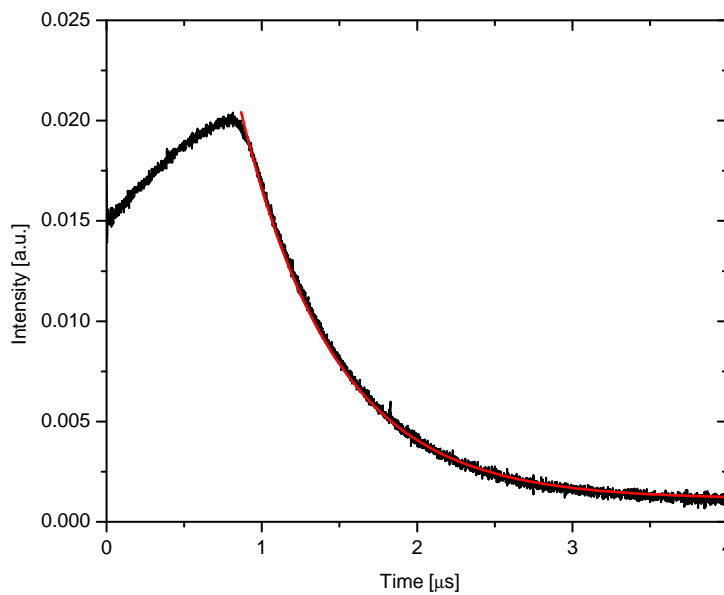

Figure 3.6: The cavity ring down measurement. Data is fitted using an exponential function with an offset. The obtained decay time is $\tau_0 = 0.601(2)\,\mu s$. An average is done on 32 measurements.

This can be determined with a reference measurement, by sending light directly to the photodiode and switching the light off in the same fashion. This value has to be subtracted from the ring down decay time

$$\tau_d = 31.0(3)\,\text{ns}$$

which gives finally

$$\tau = 0.570(2)\,\mu s$$

The linewidth follows from Eq. 3.1.3

$$\Delta\nu = 280(2)\,kHz$$

The resulting value of the finesse at $780\,nm$ wavelength is therefore according to Eq. 3.1.4

$$\mathcal{F} = 7171(14)$$

3.4 Zero-expansion temperature determination

From the characteristics of the ULE glass it is expected that length of the spacer has a minima near room temperature. At this point the length (and therefore also the resonance) of the cavity is least sensitive to temperature variations. Therefore one wants to determine the temperature value and keep the cavity at it. However, since the mirrors are made of BK7-substrate [27] which has different expansion coefficient from spacer, one can not simply take this temperature value from datasheet of ULE. The effects that come from having a different material of mirrors are described in [30]. The zero-expansion temperature of the complete cavity will be determined experimentally.
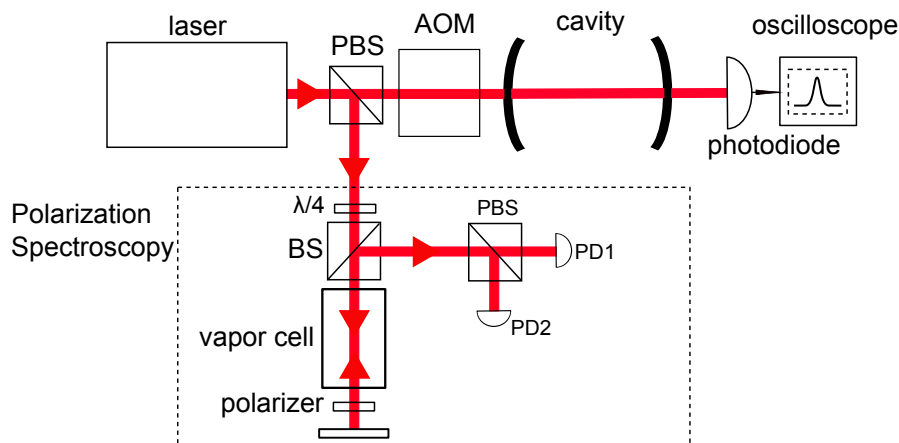
Figure 3.7: Setup for zero-expansion temperature determination. Laser is locked to the polarization spectroscopy. AOM is used to scan the frequency of light going into the cavity, such that resonance of the cavity is observed on the oscilloscope. The temperature of the cavity is then changed causing the drift of the resonance on the oscilloscope screen. This drift is then monitored.

This is done by changing the temperature of the cavity in large steps ($1\,°C$) and observing the shift of resonance comparing to an atomic reference, polarization spectroscopy [24] in this case. The polarization spectroscopy is a Doppler free technique, that can produce a dispersive signal

suitable for a laser locking. For this purpose, two counter propagating laser beams are sent through a vapor cell. A strong circularly polarized pump beam induces non uniform population of m_F states, which causes birefringence of the medium. A weak linearly polarized (superposition of σ^+ and σ^-) probe beam is counter propagated and detected with a differential photodiode. This photodiode has a polarizing beam splitter inside, so that the intensity of light of both polarizations are separately detected. The difference of two represents the error signal (Figure 3.8) to which laser can be locked.
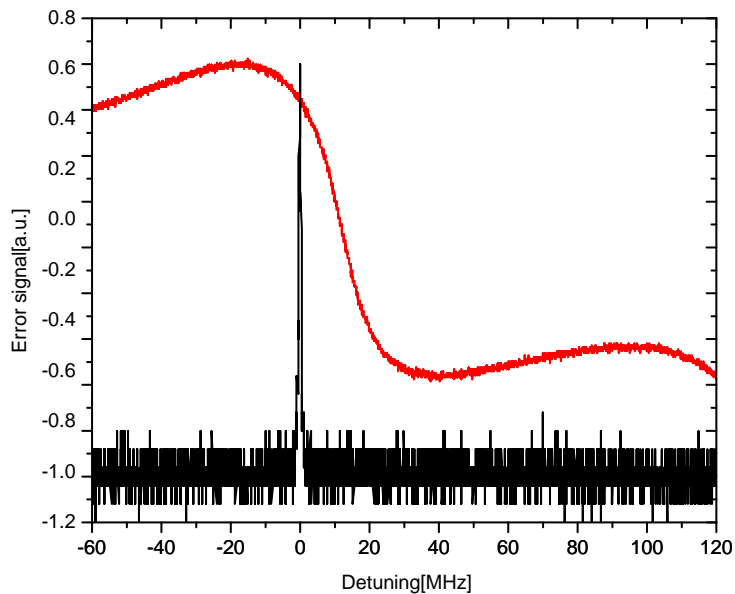

Figure 3.8: Polarization spectroscopy error signal (red) and cavity transmission (black). During the measurement the laser is locked to the slope of red signal, whereas the position of transmission resonance is recorded on the oscilloscope.

The setup is shown in Figure 3.7. The measurement procedure is following. The laser is locked to the polarization spectroscopy. Light transmitted through the cavity is detected with a photodiode. The frequency of the AOM is scanned such that the resonance signal is detected on the photodiode. Now the temperature of the outer aluminium box is changed. This will induce slow change of temperature and length of the cavity. Therefore resonance signal on the photodiode will slowly shift. This drift of the resonance feature is monitored on the oscilloscope. Bandwidth of AOM needs to be big enough to cover the range the cavity resonance is drifting. Figure 3.9 shows cavity resonance dependence on its temperature. The zero-expansion temperature is given by position of maximum of the quadratic fit curve:

$$T = 7.68(15)\,°C$$

.

The error estimation for the temperature value was taken from the error of the fit. It should be noted that the thermistor has not been calibrated absolutely. The temperature values have been converted from the measured resistance values using the datasheet of the thermistor. For this reason there could be significant systematic offset in the provided value. Assuming that the temperature of the cavity is less than $0.2\,°C$ away from zero expansion temperature this gives rise to a temperature sensitivity of less than $150\,\mathrm{kHz}\,\mathrm{K}^{-1}$. Since the temperature stabilization for the cavity is on the order of $10\,\mathrm{mK}$ this result agrees with the planned long term frequency stability of the reference.
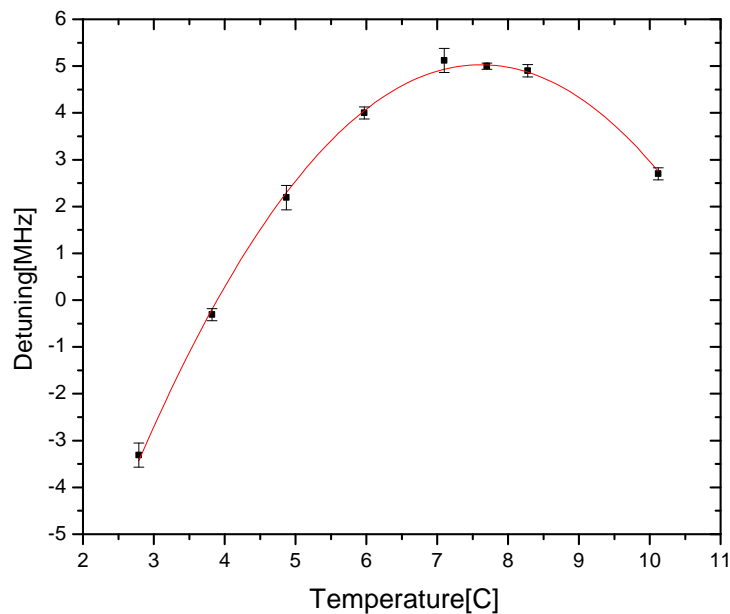

Figure 3.9: Detuning of the cavity resonance with respect to the polarization spectroscopy as a function of the cavity temperature. The fit is given by $f(T) = -0.36T^2 + 5.53T - 16.03$. At each temperature value, data is averaged and the rms of that data results in the error bars.

Locking of a diode laser at 780 nm

Once a stable reference is established, a method for comparing the laser frequency to the reference is needed. The method has to give information on what side of cavity resonance the laser is, so an appropriate correction signal can be sent to the laser. Let's assume the laser is at the exact resonance of the cavity. If its frequency changes, it will produce a change in the signal at a photodiode that is detecting light reflected from the cavity. The problem is that this signal does not provide information in what direction the frequency of the laser has changed, so using this as an error signal is not possible. Although, it is possible to operate at the side of the resonance (side of fringe locking), because here one can determine direction of the frequency change. But this method has drawbacks such as light intensity sensitivity and small bandwidth.

4.1   Pound Drever Hall lock

Ideally, one would like a dispersive cavity signal around the resonance as an error signal for the laser locking. Such a signal can be produced using the Pound-Drever-Hall (PDH) technique [31], shown in Figure 4.1.

PDH uses the fact that the phase of light reflected from the cavity behaves dispersively around the cavity resonance (Figure 3.1). For this purpose, the laser beam that is coupled into the cavity is phase modulated, so that sidebands in the frequency domain are produced. Light that is reflected from the cavity is observed with a photodiode, that is fast enough to detect the beating signal of the carrier and the sideband fields. Since the sidebands are far from the cavity resonance they serve as a phase reference. The information on the relative phase is retrieved by mixing the detected signal with the modulation signal. The resulting signal has frequency components at dc and twice the modulation frequency. The low frequency part contains the dispersive signal of the cavity resonance that can be used for locking, whereas high frequency part is removed usig low pass filter. A mathematical description is required in order to see how the exact shape of error signal arises using this method (Appendix 8.1). The advantage of the PDH technique is that it is insensitive to variations of the laser intensity. Also, since it uses light reflected from the cavity, it has a large bandwidth. The cavity does not need to be polarization sensitive, in contrast to the Hänsch-Couillaud locking scheme (cf. Section 5.2).
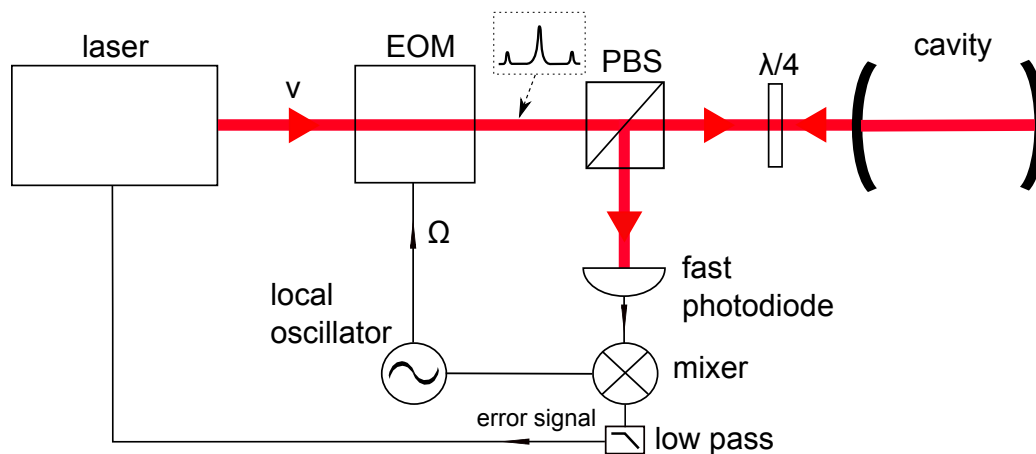
Figure 4.1: Pound Drever Hall setup. The EOM phase modulates the beam. PBS and the quarter wave-plate are used so the reflected beam can be separated from the incident beam and separately detected. The detected signal is mixed with the original modulation and low-pass filtered, producing an error signal, which is sent both to the piezo and current of the laser. A VCO is used as a local oscillator.
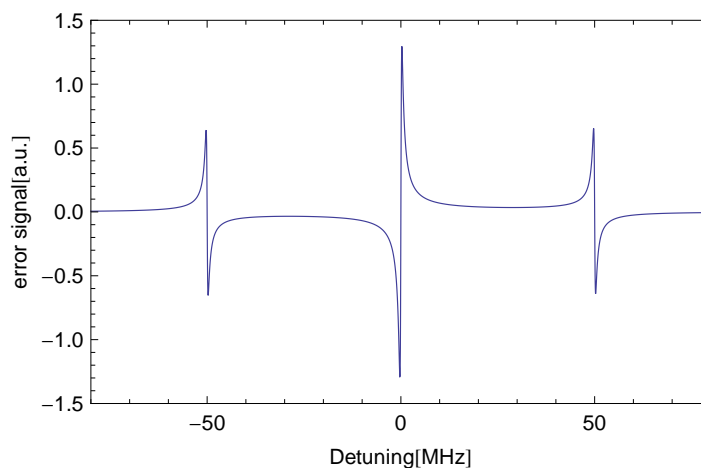

Figure 4.2: PDH error signal for modulation frequency of 50MHz. Cavity parameters are $\Delta\nu_{fsr} = 2000\,\text{MHz}$, $r = 0.9996$, which corresponds to our cavity. The derivation of this signal is give in Appendix 8.1.

4.2 Experimental setup

The laser beam is modulated using a home built EOM (see Appendix 8.3) with a resonance frequency at 47 MHz. Together with the mixer and additional electronics (amplifier, voltage controlled attenuator) it is soldered onto a single circuit board (see Appendix 8.2). The power of the light coupled inside the cavity is around $100\,\mu\text{W}$. High powers can cause heating of the mirrors and therefore fluctuations of the resonance. The reflected light is detected with Thorlabs PDA10A photodiode, that has a bandwidth of 150 MHz. The error signal after the mixer and

the low pass, obtained by scanning the laser, is shown in Figure 4.3. The signal is sensitive to the relative phase of the the modulation and detection signal and it should be optimized such that the maximum slope is achieved. The phase is adjusted by changing the length of the cable between the oscillator and the EOM.
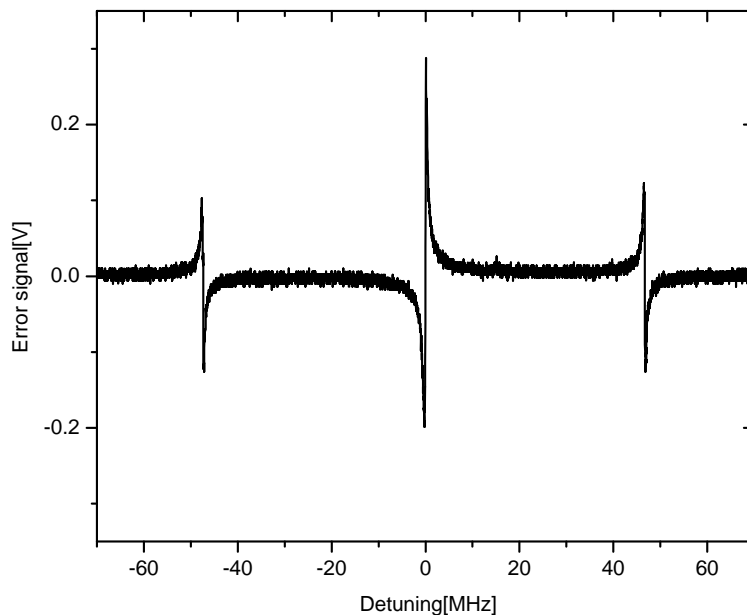

Figure 4.3: Pound Drever Hall error signal obtained by scanning the laser. The central feature corresponds to carrier, and other two features come from sidebands. These two can also be used for locking, but they have smaller slopes.

4.3 Laser feedback

After setting the method that produces the error signal, a proper feedback needs to be built, that will use the error signal to correct the lasers frequency. This is done by shaping the gain and the phase of error signal at different frequencies. High gain should be provided at low frequency, since most of noise is there. Above a certain frequency the phase of feedback becomes larger than 180°. This determines a bandwidth of the feedback loop. If the gain at this frequency is larger than one, positive feedback will occur and a system will start self oscillating. Shaping of the gain and the phase of the feedback is done by passing the error signal through the various electrical filters.

A diode laser has two different elements that can be used to change its frequency. One way to compensate frequency changes of the laser is to apply error signal to the piezo of the laser, which changes the external cavity length of the laser and as a consequence, the frequency of the laser is

changed. The bandwidth of the piezo is usually only few kilohertz, so it can not compensate for fast fluctuations. These high frequency fluctuations can be compensated by sending a feedback to the current modulation input of the laser. Therefore the signal is separated into a slow and a fast path. The slow path of the error signal goes through PI (Proportional-Integral) controller and then is fed back to the laser piezo. The integral part ensures that the gain is larger at lower frequencies. The phase and the overall gain of the fast path are adjusted with a self-built lead−lag compensator (design can be found in [32]) and applied to the laser current. Shifting the phase at high frequency with the lead−lag filter should increase the bandwidth of the feedback. The laser has a high pass filter at the input of its current modulation (cut-off frequency of around few hundred Hz), therefore this feedback works only at higher frequencies. The transition between two feedback mechanisms should be smooth, so that there is no band gap with weak or no feedback. Looking at the noise spectrum of PDH photodiode when system is locked, one can see servo bumps (frequencies that can not be efficiently compensated by the feedback). The feedback can be optimized by adjusting the values for the capacitors and the resistors in the lead−lag compensator. This way one can decrease the servo bumps and also shift them away from the central frequency, thereby increasing the bandwidth of the lock.
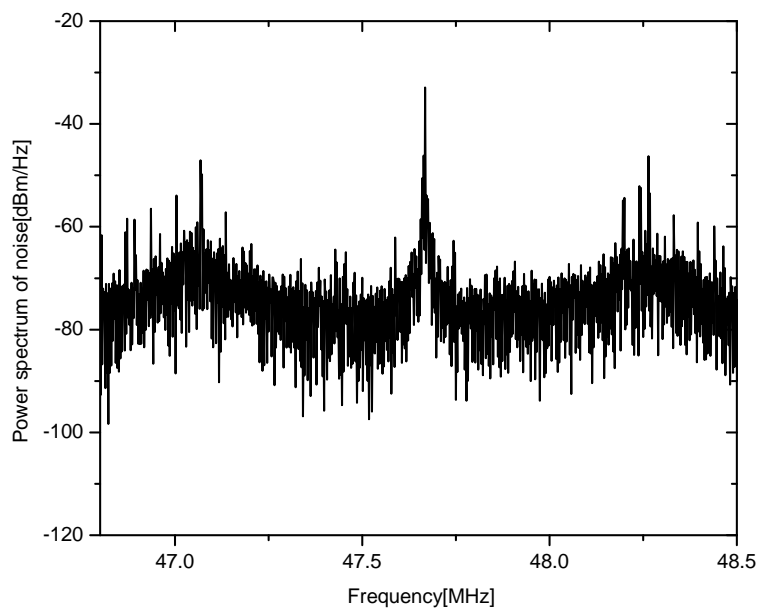

Figure 4.4: Power spectrum of the photodiode signal before the mixer, taken while the laser is locked. The resolution bandwidth is $620\,\mathrm{Hz}$. The servo bumps are around $0.6\,\mathrm{MHz}$ away from central frequency.

4.4   Linewidth of the laser

It is important for all lasers in this setup to have a narrow linewidth in order to enable coherent Rydberg atom experiments. Therefore the linewidth of the locked laser needs to be measured. There are several established methods to characterize the linewidth of a laser. One way is to beat the laser with another independent laser that has similar or better stability. Since no other laser system is available, this method is not an option. Another option is the delayed self-heterodyne method [33]. For this method one needs an optical fibre of length larger than the coherence length of laser. For a laser with linewidth of 10 kHz this requires around 10 km of optical fiber. However, a lower estimate for the laser linewidth can also be directly obtained from error signal of the lock. This gives the linewidth value comparing to the cavity, or to say it is assumed that the cavity resonance has absolute stability. So this method is a measure of the lock performance. By measuring the slope of the Pound Drever Hall error signal and the rms of the locked signal (Figure 4.3), one can estimate the linewidth as

$$\Delta\nu_L = \frac{rms}{slope} = \frac{30.5 \text{ mV}}{4.06 \text{ V/MHz}} = 7.5(3) \text{ kHz} \qquad (4.4.1)$$

According to the discussion in Chapter 2, this value matches the requirements for the coherent excitation to the Rydberg states.

Laser light at 480 nm

The 780 nm laser described in previous section will be used for excitation to $5p_{3/2}$. In order to address Rydberg states, 480 nm light is needed. In this setup it is being produced by frequency doubling the diode laser at 960 nm using a non-linear crystal inside an enhancement cavity. This method is chosen because there are no reasonably priced single mode high power laser diodes at 480 nm and we already had the cavity at our disposal. Another reason is the large tuning range, that is needed to address different Rydberg states (around 5 THz difference between n=25 state and n=70). The basics of frequency doubling will be first presented, followed by the experimental realization.

5.1   Second harmonic generation

Passing light of frequency ω through a non-linear media can generate light at frequency of 2ω. This effect is known as the Second Harmonic Generation (SHG) or the frequency doubling.

Some intuitive picture of this process is showed in Figure 5.1. Two photons of frequency ω(pump) passing through a non-linear crystal are converted into a single photon at 2ω. Quantitatively SHG can be described by using the Lorentz-oscillator model with an additional anharmonicity [34]. This yields a nonlinear dependence of medium polarization on applied electric field, causing the polarization to have a part that oscillates at twice the frequency of that field. In this model the intensity of doubled light as a function of the travelled distance through the crystal (l) is given by [34]

Figure 5.1: Left: Second harmonic generation. Right: Definition of the phase mismatch (Δk).

$$I(2\omega_1, l) \propto \left(\frac{\sin{(\Delta k l/2)}}{\Delta k l/2} \right)^2 I^2(\omega_1). \tag{5.1.1}$$

Here, $\Delta k = k(2\omega_1) - 2k(\omega_1)$ is the phase mismatch. Therefore the intensity is maximized when $\Delta k = 0$ (so called phase-matching condition). This can be also seen as a condition for the second harmonic waves created at different positions of the crystal to constructively interfere. Also, one
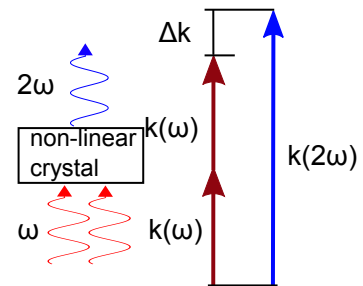
27

can write

$$\Delta k = \frac{2\omega_1}{c}(n(2\omega_1) - n(\omega_1))$$

where n is refractive index of the crystal.

Therefore the phase-matching condition will be satisfied when $n(2\omega_1) = n(\omega_1)$. In isotropic materials usually $n(2\omega_1) \neq n(\omega_1)$ holds, but one can use birefringent crystals to avoid this problem. These crystals the have property that different light polarizations have different refractive indices. It is possible to choose a direction of propagation such that an extraordinary at ω and an ordinary beam at 2ω have same index of refraction. Figure 5.2 illustrates this type of phase matching.
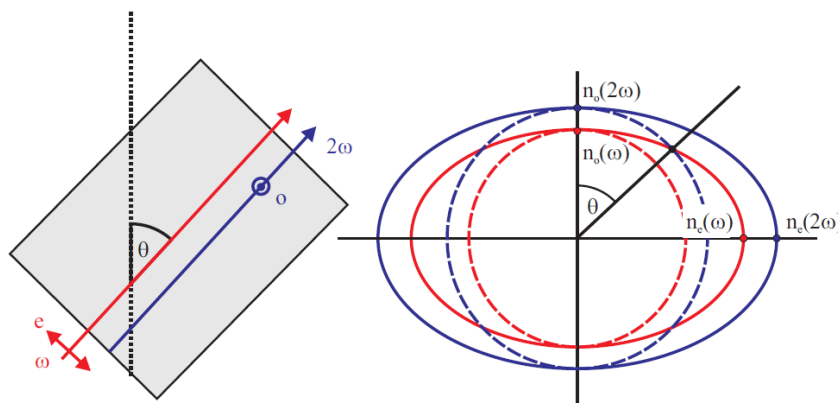

Figure 5.2: Birefringent phase matching. The light fields are chosen to propagate at angle Θ with respect to optical axis (dashed). The ideal angle is determined by cross point of red ellipse (extraordinary index of refraction) and blue circle (ordinary index of refraction). The Figure is taken from [28].

Besides phase matching, in order to get a good conversion efficiency, the crystal is usually placed inside an enhancement cavity (resonant for pump field). In this way unconverted light can pass through the crystal many times. This build up of the intensity of light at ω, increases the power at 2ω drastically because of the quadratic dependence (Eq. 5.1.1). For this purpose, the length of the enhancement cavity must be locked to the laser so that the doubling cavity is always resonant with the laser light. Doubling cavities usually have piezo on one of the mirrors so its resonance (length) can be adjusted to match the pump light frequency. There are several other things that one should take into account for frequency doubling. An important role is played by the optimal focusing conditions into the crystal. This can be calculated using Boyd-Kleinmann theory [35]. Another consideration is the impedance matching of the light into the cavity in order to couple the maximum amount of power into cavity. The impedance is optimally matched when the incoupling mirror transmits same amount of light as it is lost inside cavity.

5.2 Experimental setup of frequency doubling

A schematic of the experimental setup for generating light of 480 nm light. The light from a home-built external cavity diode laser in Littrow grating configuration at 960 nm is frequency doubled in a resonant Bow-tie cavity. For SHG, a BIBO crystal (3x3x10 mm) is used. The crystal and the enhancement cavity had previously been used in our group for frequency doubling 980 nm light as a part of atomic indium experiment. The design of the cavity, including impedance matching and optimization of the Boyd-Kleimann parameters are detailed in [36]. We have verified that the design is adequate for SHG at 960 nm. I had to reassemble the cavity and to optimize it for 960 nm light.

Since the efficiency of frequency doubling scales linear with pump light power, it is important that a good coupling into the cavity is achieved. For this purpose, a telescope of cylindrical lenses is used to reshape the elliptical beam of the diode laser. In addition to that, two more spherical lenses are used to set the size of the waist of the beam at a proper position. The achieved coupling efficiency is around 0.75. The crystal inside the cavity is placed on a rotational stage, so the phase matching condition can be adjusted.
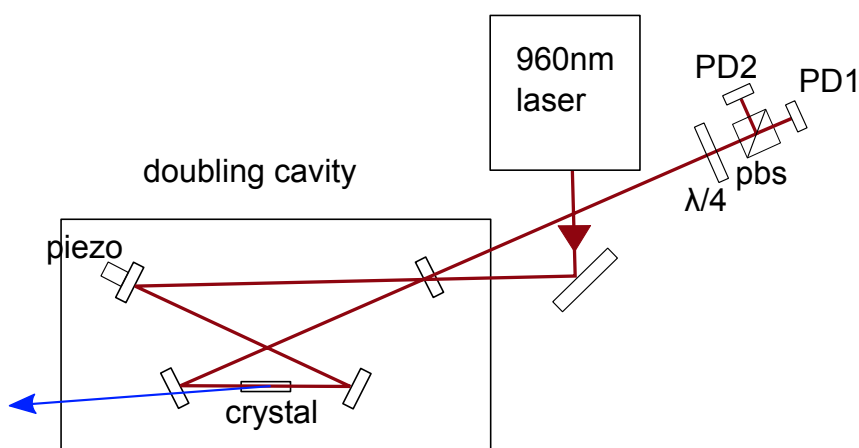

Figure 5.3: Bow-tie enhancement cavity with Hänsch-Couillaud locking setup. Error signal is obtained from difference of signals detected with photodiodes (PD1 and PD2). Optics used for beam shaping and mode matching are not on the figure.

Additionally the crystal is surrounded with a copper shield whose temperature can be adjusted with a Peltier element. Since the indices of refraction also depends on the temperature, this enables fine tuning of the phase matching.

In order to keep the enhancement cavity resonant with the light at 960 nm, it needs to be frequency locked to the laser. One of the cavity mirrors is attached to a piezo actuator such that the length (resonance) of the cavity can be tuned. The free spectral range of the cavity is 386 MHz and the finesse is around 100. To produce the error signal for this lock, the Hänsch-
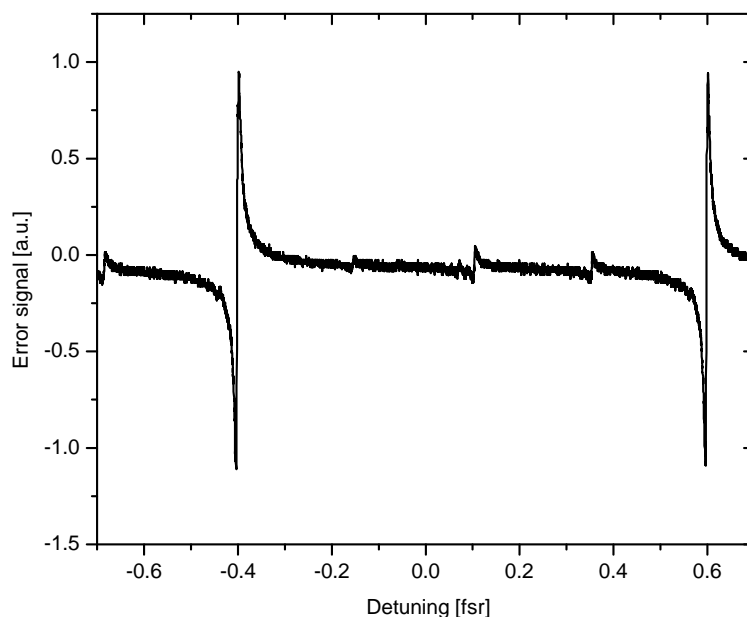
Figure 5.4: Hänsch-Couillaud error signal. Smaller dispersive signals corespond to higher order modes of the cavity.

Couillaud locking scheme is used [37]. The basic idea of this lock is to detect the ellipticity in the polarization of light reflected from the cavity. Because of the birefringence of the crystal, the cavity is resonant only for one polarization. Depending on the resonance condition, the reflected light of this polarization will gain a detuning dependent phase and as a result the ellipticity will change. The polarization of the incident beam has to be set such that some of the light does not have proper polarization to be coupled into the cavity. This non-resonant polarization serves as kind of a phase reference. The error signal (Figure 5.4) is fed back through PI controller to the cavity piezo. In this case the cavity is locked to the laser, and laser will be eventually locked to a further spectroscopic reference. During early stages of the experiment we observed strong fluctuations in the output power of the cavity. An additional isolator had to be placed before the doubling cavity because there were some reflections from cavity, going back to the laser and making the laser lock unstable. Due to a big walk off angle of the BIBO crystal, mode of blue light produced by doubling cavity has a poor quality (elliptical with some sidemodes). A similarly bad beam quality with BIBO was also observed in Kim's thesis. Cylindric lenses (75mm and 300mm) are placed after cavity in order to shape the beam. To quantify the beam quality, the light is coupled into a single mode fiber and we achieve a coupling efficiency of around 0.55. One can consider using a crystal with a smaller walk off angle. A BBO crystal was also at our disposal, but that one has a significantly smaller conversion efficiency [36].

Around 50 mW of 960 nm light are coupled into cavity. At this pump power, currently an output power of up to 0.8 mW is achieved. Due to a small value of the transition matrix elements for
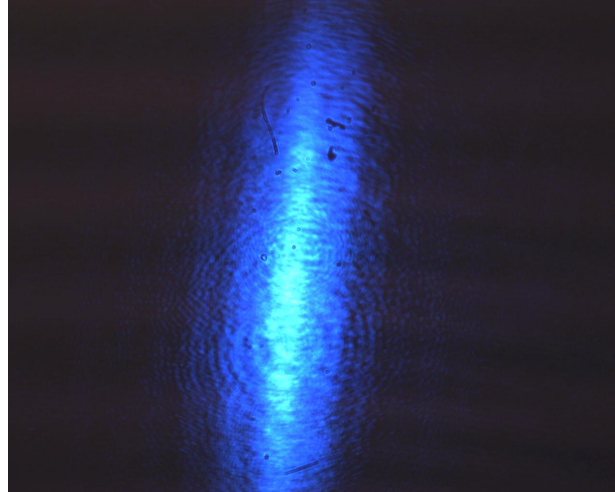
Figure 5.5: Profile of the blue beam exiting the doubling cavity. Circles and black dots are artifacts of the camera which is used for imaging. Using two cylindrical lenses the beam was shaped such that around 0.55 of power was coupled into a single mode fiber.

an excitation into the Rydberg states, a power on the order of $100\,\mathrm{mW}$ is needed for planned experiments (Section 2.3). Therefore a tapered amplifier should in the future be added to increase the pump power before the frequency doubling cavity. With tenfold increase in the pump power, approximately a hundredfold increase in power of blue light should be achieved. Preforming EIT (Chapter 6) in a vapor cell and should be possible with this power [38].
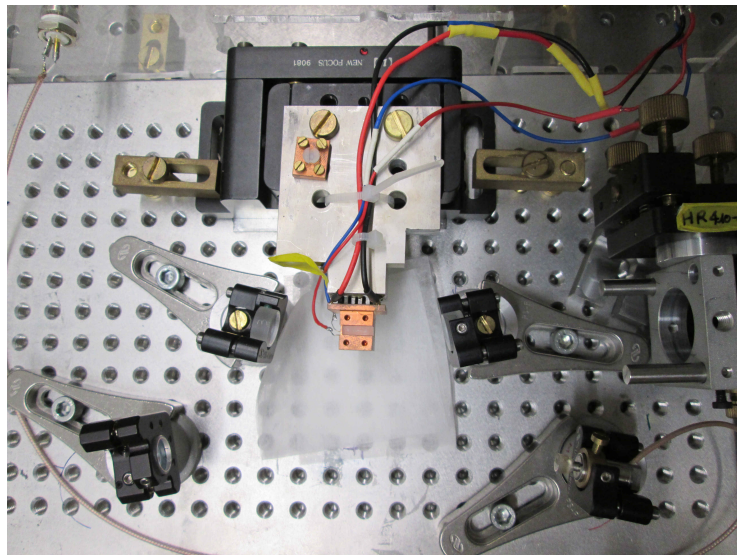

Figure 5.6: Image of the frequency doubling cavity. Pump beam enters cavity through down left mirror which has a lower reflectivity. The mirror in the upper right corner is transparent for blue light and that is where the blue beam exits the cavity. The mirror in the lower right corner has a piezo for adjusting the length (resonance) of the cavity.

Rydberg Electromagnetically Induced Transparency (EIT)

In previous chapters, we have described the setup for generation of laser light fields needed in the two-photon excitation scheme. In this chapter, we will demonstrate that this laser system can indeed achieve the coupling to Rydberg states in ^{87}Rb atoms. The most obvious way to demonstrate this would be to resonantly drive Rydberg transition and subsequently detect population in the Rydberg state. This is not a convenient approach for the atoms at room temperature in a vapor cell. Instead, EIT[1] spectroscopy is performed [41].

In addition, we are interested in EIT spectroscopy because it can be used for locking the laser at 480 nm. An error signal can be obtained using frequency modulation technique [38]. First, theory of EIT will be outlined here and then the experimental realization in a vapor cell will be presented.

6.1   Qualitative description of Rydberg EIT

EIT is a phenomena, where a narrow transparency window is opened in the resonant light absorption profile of a medium. This effect happens due to a presence of an additional light field that couples excited state of medium with an additional third state. Therefore, EIT requires at a least three level system. A detailed review of EIT is given in [42]. In the case of Rydberg excitation, the system is in a ladder configuration (Figure 2.2). In the following, red light will be referred to as probe and blue will be called coupling light. The transition from the ground to the Rydberg state is dipole forbidden. In the picture of bare states, EIT can be explained in following manner. There are two paths electron can be excited from ground to intermediate state. One is direct absorption of a photon ($|5s\rangle \rightarrow |5p\rangle$). Another path is absorption to intermediate state, then absorption to the Rydberg state and finally stimulated emission to intermediate state ($|5s\rangle \rightarrow |5p\rangle \rightarrow |Ryd\rangle \rightarrow |5p\rangle$). These two absorption paths can destructively interfere and reduce the probability for absorption of photons. This interference between different excitation channels is often called Fano interference.

---

[1]Because of the high optical non-linearity that it produces, EIT, itself is a topic that is being extensively explored [39]. The EIT and Rydberg blockade can be combined to achieve strong photon photon interaction [40].

6.2   Quantitative description of Rydberg EIT

The basics of atom light interaction for two level systems can be found in many textbooks (for example [43]). Here, we will need to extend this to three level systems. A semiclassical description will be used, in which the atom is treated quantum mechanically and light classically. The density matrix approach is more general than the single atom wavefunction description and it can model processes such as spontaneous emission and dephasing. The derivation presented here closely follows the treatment of references [42, 44].

We use the notation for the atomic levels shown in Figure 2.2. The total Hamiltonian (H) of the system can be split into the atomic Hamiltonian (H_0) and the Hamiltonian describing the interaction of the three level atom with the probe and coupling fields (H_{int})

$$H_0 = \hbar(\omega_1|1\rangle\langle1|+\omega_2|2\rangle\langle2|+\omega_3|3\rangle\langle3|)$$

$$H_{int} = -\frac{\hbar}{2}\left(\Omega_p e^{-i\omega_p t}|1\rangle\langle2|+\Omega_c e^{-i\omega_c t}|2\rangle\langle3|\right) + \text{h.c.},$$

where Ω_p, Ω_c are probe and coupling field Rabi frequencies and ω_p, ω_c are their respective frequencies detuned by $\Delta_1 = \omega_p - \omega_{21}$ and $\Delta_2 = \omega_c - \omega_{32}$. The matrix form of the full Hamiltonian in the rotating frame can be written as [42]

$$H = \frac{\hbar}{2}\begin{pmatrix} 0 & \Omega_p & 0 \\ \Omega_p & -2\Delta_1 & \Omega_c \\ 0 & \Omega_c & -2(\Delta_1 + \Delta_2) \end{pmatrix}$$

Here, the zero energy level is set to be the energy of the state $|1\rangle$. The coherent time evolution of the density matrix (ρ) is given by

$$\dot{\rho} = -\frac{i}{\hbar}[H,\rho]. \tag{6.2.1}$$

However, this equation does not include the effects of spontaneous emission or the dephasing processes, that occur due to atom collisions and technical fluctuations. Here, we will consider only spontaneous emission. Eq. 6.2.1 can be modified such that these effects are phenomenologically included in the Liouville equation

$$\dot{\rho} = -\frac{i}{\hbar}[H,\rho] + \mathcal{L}, \tag{6.2.2}$$

where [43]

$$\mathcal{L} = -\frac{1}{2}\begin{pmatrix} -2\Gamma_2\rho_{22} & \Gamma_2\rho_{12} & \Gamma_3\rho_{13} \\ \Gamma_2\rho_{21} & -2\Gamma_2\rho_{12} + 2\Gamma_3\rho_{33} & (\Gamma_2+\Gamma_3)\rho_{23} \\ \Gamma_3\rho_{31} & (\Gamma_2+\Gamma_3)\rho_{32} & 2\Gamma_3\rho_{33} \end{pmatrix} \tag{6.2.3}$$

The equations of motion for off-diagonal matrix elements are

$$\dot{\rho_{32}} = -(\gamma_{32} - i\Delta_2)\rho_{32} + i\Omega_c(\rho_{33} - \rho_{22}) + i\Omega_p\rho_{31} \tag{6.2.4}$$

$$\dot{\rho_{21}} = -(\gamma_{21} - i\Delta_1)\rho_{21} + i\Omega_c(\rho_{33} - \rho_{22}) + i\Omega_p\rho_{31} \tag{6.2.5}$$

$$\dot{\rho_{31}} = -(\gamma_{31} - i(\Delta_2 + \Delta_1))\rho_{32} + i\Omega_c(\rho_{33} - \rho_{22}) + i\Omega_p\rho_{32} \tag{6.2.6}$$

where $\gamma_{ij} = (\Gamma_i + \Gamma_j)/2$ and $\Gamma_{i,j}$ are decay rates of the states i, j. These equations can be solved in the limit of a weak probe beam ($\Omega_p \ll \Omega_c$). In this case $\rho_{33} = \rho_{22} \simeq 0$ and the solution is given by

$$\rho_{21} = \frac{i\Omega_p/2}{\gamma_{21} - i\Delta_1 + \frac{\Omega_c^2/4}{\gamma_{31} - i(\Delta_1 + \Delta_2)}}. \tag{6.2.7}$$

The electric susceptibility (χ) for probe beam can be obtained from coherences using

$$\chi = 2\frac{d_{12}^2 N_0}{\epsilon_0 \hbar \Omega_p}\rho_{12}, \tag{6.2.8}$$

where N_0 is density of atoms and d_{12} is transition matrix element between ground and intermediate state. This results in

$$\chi = \frac{d_{12}^2}{\epsilon_0 \hbar} \frac{i}{\gamma_{21} - i\Delta_1 + \frac{\Omega_c^2/4}{\gamma_{31} - i(\Delta_1 + \Delta_2)}}. \tag{6.2.9}$$

The absorption coefficient of the atomic medium is the imaginary part of refractive index ($n = \chi + 1$) as

$$\alpha = \frac{4\pi Im[n]}{\lambda_0}, \tag{6.2.10}$$

where λ_0 is wavelength of probe light in vacuum.

Figure 6.1 shows coherence ρ_{21} for different exemplary parameters. Note that when $\Omega_c = 0$, the usual Lorentzian lineshape is obtained. The linewidth feature of EIT follows the dependence

$$\Delta_{eit} \propto \frac{\Omega_c^2}{\Delta_1}. \tag{6.2.11}$$

Since here EIT will be performed in a room temperature vapor cell, the Doppler broadening due to the thermal motion of the atoms needs to be taken into account [44] as well. The shift of light frequency that a particle moving with velocity v sees, due to Doppler effect is $\omega\frac{v}{c}$. Eq. 6.2.9 can therefore be modified to

$$\chi(\Delta_1, v)dv = \frac{d_{12}^2\rho_A}{\epsilon_0\hbar} \frac{i}{\gamma_{21} - i\Delta_1 - i\omega_p\frac{v}{c} + \frac{\Omega_c^2/4}{\gamma_{31} - i(\Delta_1 + \Delta_2) - i(\omega_p\frac{v}{c} - \omega_c\frac{v}{c})}}N(v)dv \tag{6.2.12}$$

where N is the velocity distribution of the atoms. We assume a Maxwell-Boltzmann distribution

$$N(v)dv = \frac{N_0}{v_p\pi}e^{-(v/vp)^2}dv, \tag{6.2.13}$$

where N_0 is the density of atoms in the ground level, $v_p = \sqrt{\frac{2k_bT}{m}}$ is the most probable velocity, m is the mass of Rubidium 87 atom and T is temperature of the vapor. Now, one needs to integrate full expression for χ to obtain the EIT feature in vapor cell. For direct comparison with experimental data further dephasing effects due to atomic collisions and technical noise would also have to be included in a more detailed discussion. This is beyond the scope of this thesis.
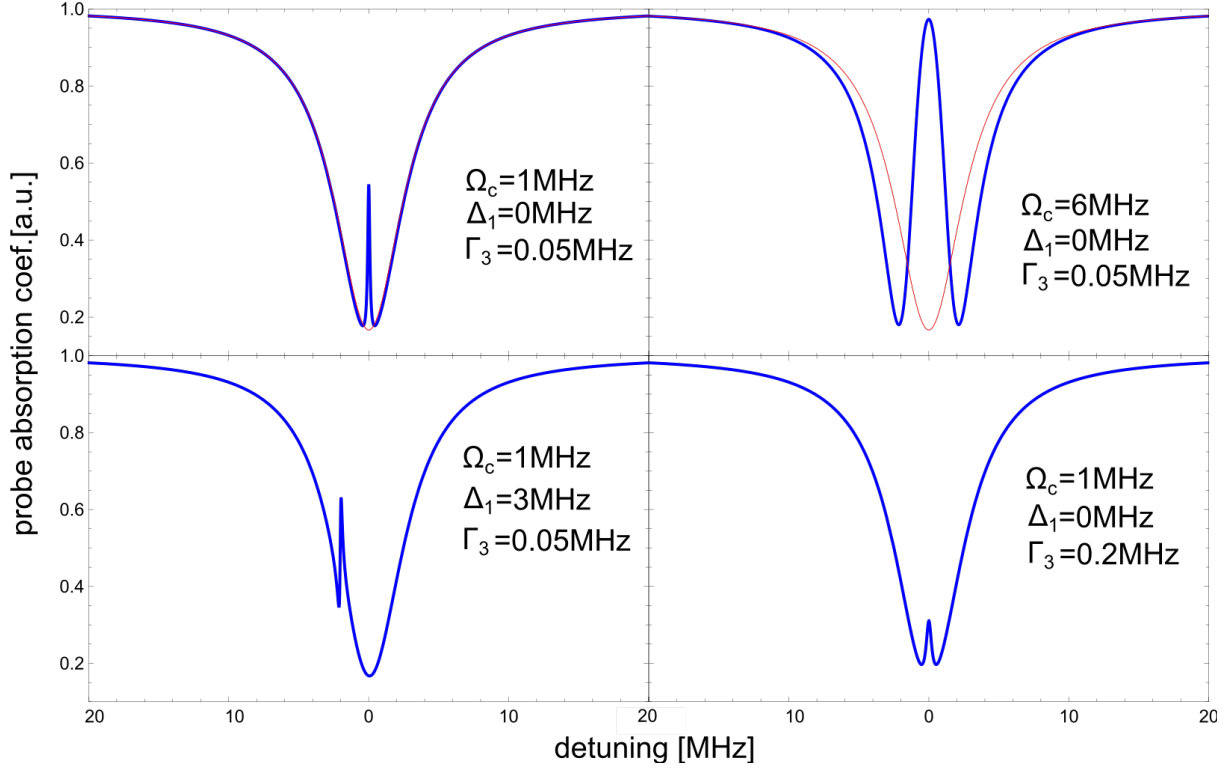
Figure 6.1: Plot of real part ρ_{21} as a function of probe beam detuning, for various parameters of coupling beam Rabi frequencies and detunings. The decay rate of the intermediate state is $\Gamma_2 = 6$ MHz, the Rabi frequency of the probe beam is $\Omega_p = 0.05$ MHz and detuning$\Delta_p = 0$. Coupling beam parameters are given in each figure as well as the assumed Rydberg state decay rate. The wavelength of the probe and the coupling beam are 780 nm and 480 nm respectively. The red line is obtained when coupling field is off, so it is natural line of the probe transition.

6.3 Rydberg EIT in a vapor cell

EIT with Rydberg atoms was first observed in [41] and locking a laser to it was first achieved in same group [38]. We closely follow their experimental configuration.

The overall setup is shown in Figure 6.2. The blue and red laser beam are counter propagated through magnetically shielded vapor cell of 10 cm length and natural isotope content. Since little of blue light is available, beams are focused in order to increase coupling to Rydberg states. The waists of both beams are around 40 µm. The red beam is detected with biased photodiode (1 MΩ resistor) after passing the cell. Its light needs to be resonant with $5s_{1/2}(F = 2) \rightarrow 5p_{3/2}(F = 3)$ transition. For this purpose we perform the saturation spectroscopy (see Figure 6.3). The laser is then locked to the nearest cavity resonance and the frequency difference to the atomic transition is bridged with a double pass AOM. Distances between peaks are proportional to difference of transition frequencies to different hyperfine states (assuming piezo non linearity is
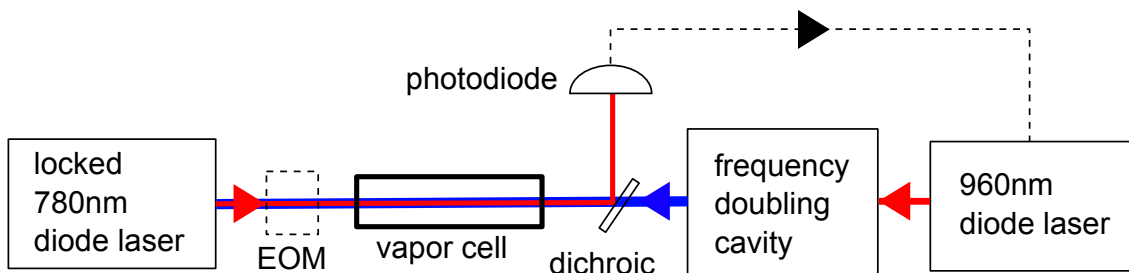
Figure 6.2: Setup for Rydberg EIT spectroscopy in a vapor cell. Phase modulation of the probe beam by an EOM can be used for obtaining the error signal, in similar fashion as the PDH technique (not done in this thesis). For this purpose the present photodiode has to be replaced by a faster one.
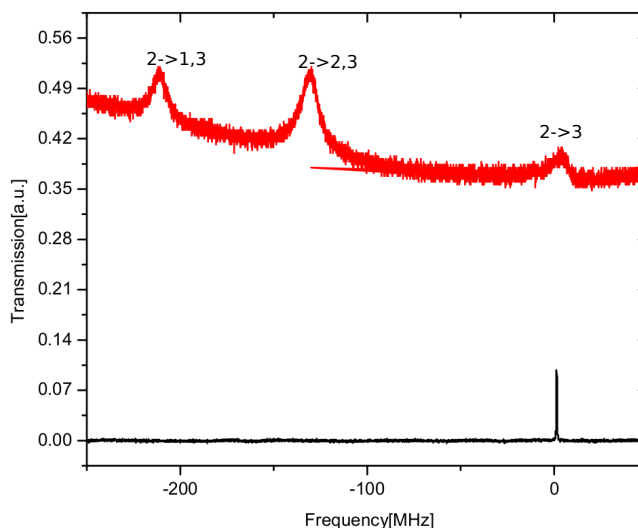

Figure 6.3: Red: Saturation spectroscopy in Rubidium cell. The peaks $2 \to 2, 3$ and $2 \to 1, 3$ are crossover peaks. Black: Transmission of the cavity. The cavity resonance is shifted with an AOM such that the laser can be locked to the $5s_{1/2}(F = 2) \to 5p_{3/2}(F = 3)$ transition.

negligible). Using this we can identify what peaks correspond to what transitions. The blue laser is adjusted to approximately the $5p_{3/2} \to nd_{5/2}$ transition using the wavemeter. The values for the frequencies of the Rydberg transitions are taken from [45]. The blue laser is then scanned in range of around 100 MHz and the center frequency is slowly shifted in order to find EIT resonance.

An absorption spectra is given in Figure 6.4. When the blue laser is scanned over the resonance, the medium becomes more transparent for the red light, increasing the amount of the red light passing through the cell.

The polarization of both beams is initially set to be circular, and later it is optimized by rotating quarter wave plate to get the largest EIT signal.
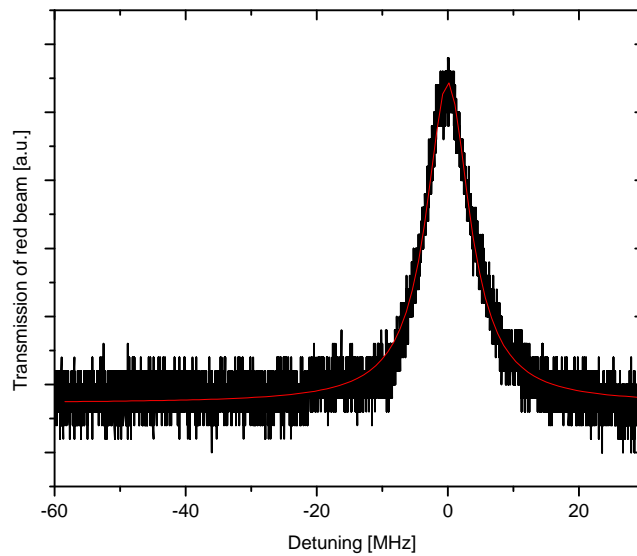
Figure 6.4: Rydberg EIT using the $26d_{5/2}$ state. Fitting with Lorentzian gives a linewidth of $\Delta\nu_{EIT} = 8.0(4)$ MHz. The red probe laser is locked to $5s_{1/2}(F = 2) \rightarrow 5p_{3/2}(F = 3)$, while the blue coupling light is scanned over the resonance. The powers of red probe and blue coupling laser beams are $3\,\mu$W and $600\,\mu$W, respectively. The height of the peak is around a few percent of Doppler broadened absorption depth.

As n number increases, the transition matrix element decreases. Transitions to s states have much smaller transition matrix elements so more power is needed. Therefore with this setup the best signal can be obtained for low lying d states.
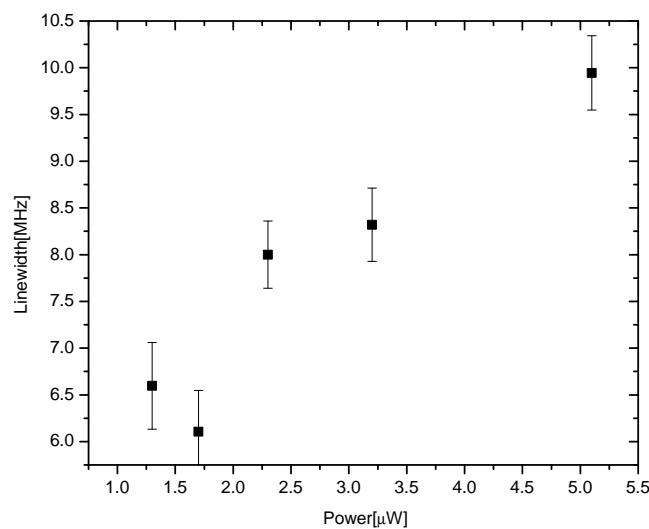

Figure 6.5: The linewidth of EIT feature as a function of the probe beam power.

Preliminary investigation (Figure 6.5) suggests that the EIT linewidth is dominated by power broadening of the probe beam. We could make the EIT feature narrower, since Eq. 6.2.11 shows that the weaker the coupling beam, the narrower the EIT feature gets, but also the peak value gets smaller and our EIT signal is already quite weak. Optimization of the relevant parameters (focusing, beam power) should be done once an error signal of EIT is produced by frequency modulation of the probe beam. At that point the spectroscopy signal should be optimized for maximum slope of the error signal, rather than narrowness of the EIT feature.

The drawback of this method is that it requires a lot of power of blue light, especially for high lying Rydberg states. Locking to a cavity in the same fashion as for the red laser is probably a better option. Despite that EIT spectroscopy serves as a first test for our Rydberg system. In addition the vapor cell could be heated in order to achieve higher optical density and obtain a better signal to noise ratio.

Conclusion and Outlook

In this thesis I report on the implementation of a setup that should enable experiments using Rydberg physics in our research group for the first time. By adding the capabilities of controlled Rydberg excitations to our current experiments with individual atoms in the optical cavities, we expect many new experimental possibilities (such as fast atomic entanglement generation and deterministic single photon sources with high bandwidth). In order to fully exploit the features that Rydberg atoms offer for this purpose, a setup for fast coherent excitation has to be built. My thesis represents an experimental contribution towards this goal. Having in mind the discussion of requirements for the setup, given in Chapter 2, the following things have been achieved:

- A stable frequency reference has been built by putting an ULE cavity inside a vacuum chamber

- The cavity has been characterized by measuring its linewidth and zero-expansion temperature. The measured linewidth is $280\,\mathrm{kHz}$ and zero-expansion temperature is $7.68(15)\,°\mathrm{C}$

- A diode laser at $780\,\mathrm{nm}$ has been locked to the cavity using the Pound Drever Hall method.

- We have characterized the locking by measuring the linewidth of the laser at $780\,\mathrm{nm}$ relative to the cavity to be $7.5\,\mathrm{kHz}$. Note however, that no information could be obtained on how stable the cavity itself is. For a measurement of the actual linewidth one needs to perform a self-heterodyne measurement, or compare the laser system with a further stable laser system.

- Laser light at $480\,\mathrm{nm}$ has been produced by frequency doubling light from a laser diode at $960\,\mathrm{nm}$ using a BIBO crystal inside an enhancement cavity. The setup produces around $0.8\,\mathrm{mW}$ of light at $480\,\mathrm{nm}$, which is sufficient for first proof of principle experiments, but far less than what is needed for quantum information experiments.

- Finally, with this setup we have managed to successfully address Rydberg states by performing EIT at room temperature in a vapor cell.

The next steps for this setup should include several technical improvements:

A tappered amplifier for 960 nm light should be added before doubling cavity in order to increase power of light at 480 nm.

For this purpose the laser light at 480 nm will have to be locked to the EIT spectroscopy. One can also consider locking the 960 nm laser to a modified ULE cavity, since this type of locking requires much less power.

This will give enough power to coherently excite small ensembles of ultracold Rubidium atoms to Rydberg states in our lab. One can also consider locking of the 960 nm laser to another cavity, since this type of locking requires much less power. Additionally that cavity could be used to characterize the stability of the cavity that has already been built, in case it is also resonant for 780 nm.
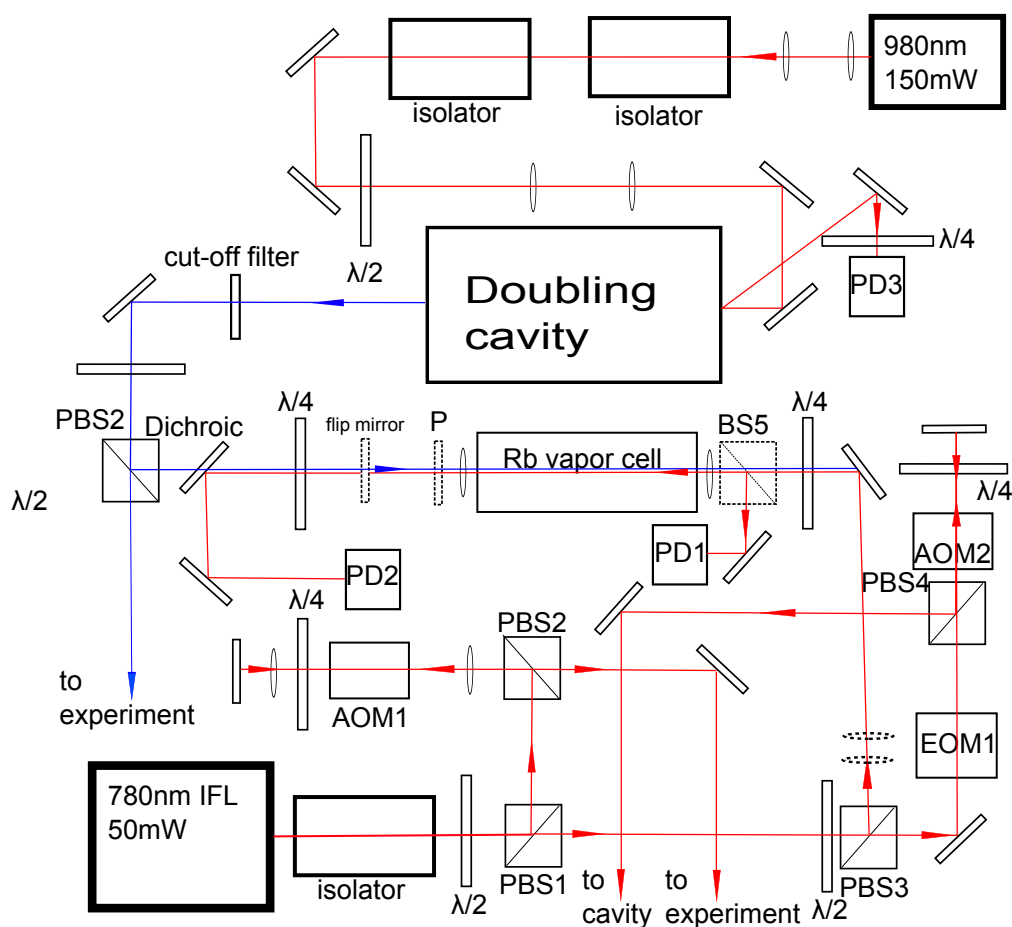

Figure 7.1: Detailed scheme of the optical part of the setup. All elements shown here are placed on one breadboard, while the ULE cavity is inside a vacuum chamber on an additional breadboard. Dashed elements have been used for performing polarization spectroscopy and they are not part of EIT setup.

Appendix

8.1 Derivation of PDH error signal

This section follows the derivation from [46] and [31].

After the laser beam is phase modulated with frequency Ω, its electric field can be approximated with

$$E = E_0 e^{i(\omega t + \beta sin(\Omega t))} \tag{8.1.1}$$

where β is called the modulation depth, and it describes strength of the phase modulation. Using Bessel functions one can rewrite previous expression as

$$E \approx E_0 (J_0 e^{i\omega t} + J_1 e^{i(\omega + \Omega)t} - J_1 e^{i(\omega + \Omega)t}). \tag{8.1.2}$$

This light is coupled into cavity and its reflection is monitored on a photodiode. The reflected field is given by

$$E \approx E_0 (F(\omega) J_0 e^{i\omega t} + F(\omega + \Omega) J_1 e^{i(\omega + \Omega)t} - F(\omega - \Omega) J_1 e^{i(\omega + \Omega)t}), \tag{8.1.3}$$

where the $F(\omega)$ is the reflectivity of cavity. The Expression for $F(\omega)$ is given in Eq. 3.1.1. Signal that photodiode detects is proportional to power of beam, which is equal to

$$\begin{aligned} P_{ref} = P_c \mid F(\omega) \mid^2 + P_s (\mid F(\omega + \Omega) \mid^2 + \mid F(\omega - \Omega) \mid^2) \\ + 2\sqrt{P_c P_s} \Big(Re[F(\omega) F^*(\omega + \Omega) - F^*(\omega) F(\omega - \Omega)] cos(\Omega t) \\ + Im[F(\omega) F^*(\omega + \Omega) - F^*(\omega) F(\omega - \Omega)] sin(\Omega t) \Big) \\ + (2\Omega \text{ terms}), \end{aligned} \tag{8.1.4}$$

where $P_c = E_0 J_0$ and $P_s = E_0 J_1$. This signal is being mixed with modulation signal. Whether the *sine* or the *cosine* part is extracted, can be adjusted by changing phase delay between the oscillator and the EOM. Mixer produces signals at DC and twice the modulation frequency. The later one is filtered out with low pass, so only DC term will survive. Additionally it is assumed that sidebands are far from resonance, so $F(\omega - \Omega) \approx -1$. Finally the error signal is given by.

$$\epsilon = -2\sqrt{P_c P_s} Im[F(\omega) F^*(\omega + \Omega) - F^*(\omega) F(\omega - \Omega)] \tag{8.1.5}$$

The optimal modulation index is $\beta = 1.08$ [46], which is corresponds $P_c/P_s = 0.42..$ The phase should be adjusted such that steepest error signal is produced in order to obtain best signal to noise ratio.
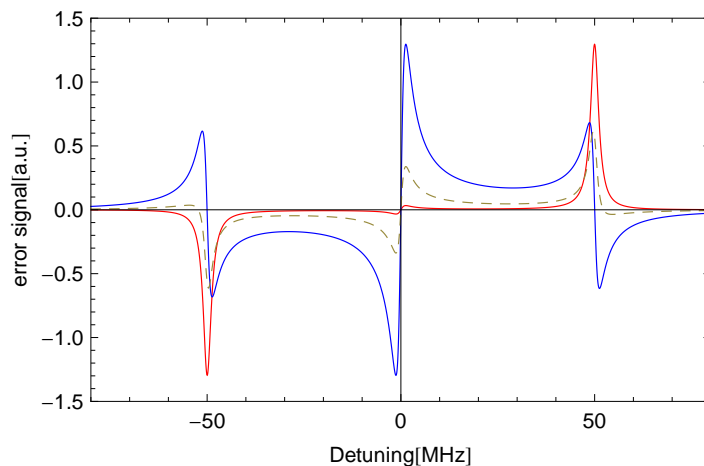
Figure 8.1: PDH error signal for various phases with modulation frequency of 50MHz. Red - zero phase (Real part), Blue - $\pi/2$ phase (Imaginary part), Dashed - $\pi/6$ phase. Cavity parameters are $\Delta\nu_{fsr} = 2000\,\mathrm{MHz}$ and $r = 0.998$. Reflection coefficient is smaller than for our cavity for graphical reasons. Derivation of this signal is give in Appendix 8.1.

8.2 PDH electronics

The oscillator (MiniCircuits POS-100) and the mixer (MiniCircuits SRA-1) used for PDH scheme were soldered on a single board (Figure 8.2) and put into metal box for shielding. Additional RF elements on the board include power splitter, amplifier and voltage variable attenuator.

8.3 Self-built EOM

For the phase modulation of the lasers, a home built EOM is used. A LiNbO˙3 crystal (from Almaz optics) with dimensions 2x2x20 mm is mounted between copper foil electrodes. The crystal behaves as capacitor and it is connected to a self wound copper coil inductor to form a resonant LC circuit. Its resonant frequency is given by

$$\nu_{eom} = \frac{1}{2\pi\sqrt{LC}}$$

where L is inductance of the inductor and C capacitance of the crystal. RF power into this circuit is coupled inductively by means of an additional coil (see Figure 8.4). This resonant EOM will produce significant modulation only when driven close to its center frequency ν_{eom}. In order to have optimal modulation index for PDH at 780 nm, it is necessary to input around 22 dBm of resonant RF power. One can calculate ν_{eom} value, but because of imperfections of inductor (solenoid), it is better to experimentally. An additional pick-up coil in the EOM is used just for characterising EOM. Connecting the two coupling coils to output and input of network analyser, the transfer function of EOM can be obtained. This gives us the exact resonance frequency and the quality factor of EOM. The measured transfer function of EOM is shown in Figure 8.5.
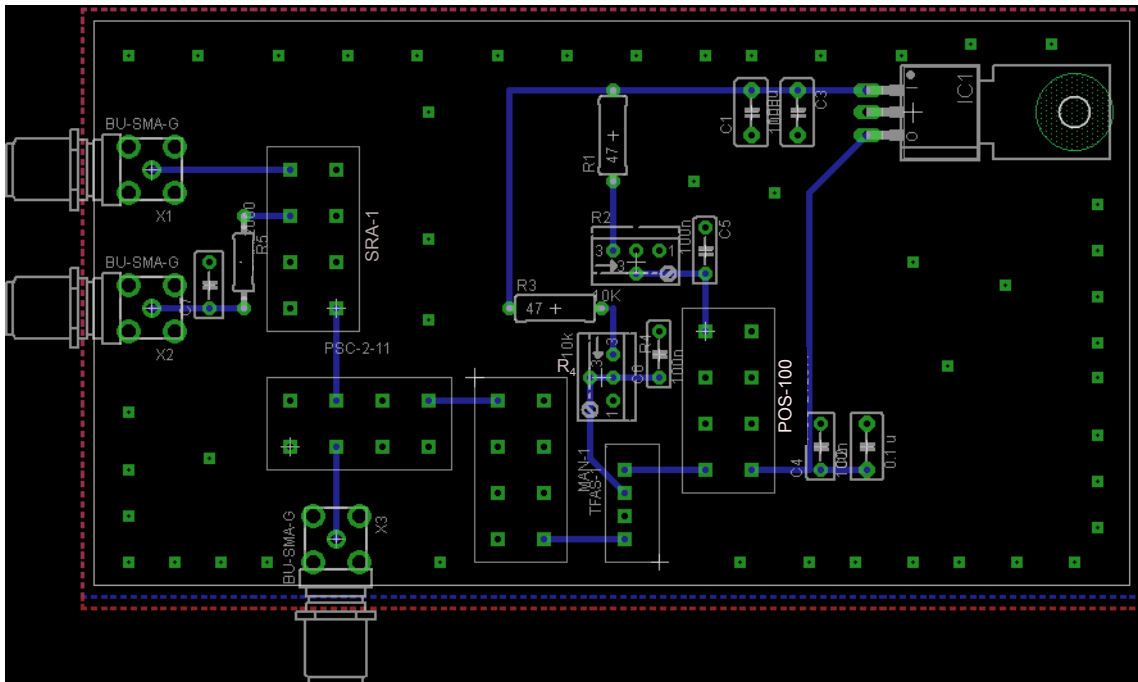
Figure 8.2: PDH electronics board. Potentiometer R_2 is used to control the frequency of the output of the VCO (POS-100) and potentiometer R_4 to control the output power of circuit by controlling the attenuation at VCA (TFAS-1). The RF signal is amplified using MiniCircuits MAN-1 and power split (using MiniCircuits PSC-2-1) such that one part is used for driving EOM (additional amplifier is neded in between) and rest for mixing with photodiode signal (X1 input)
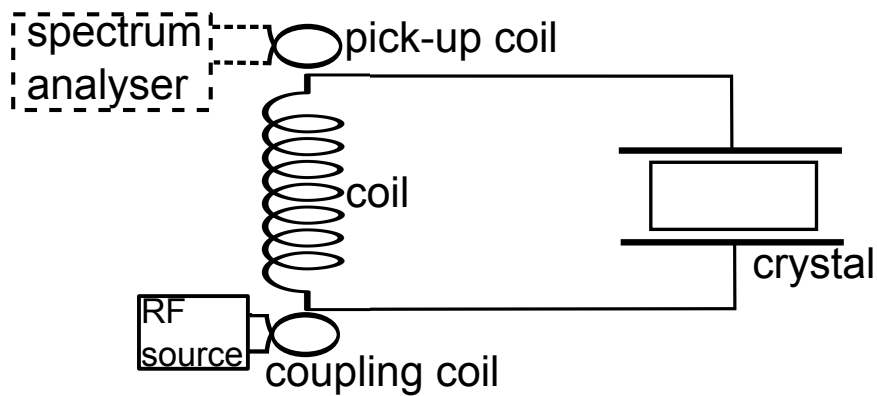

Figure 8.3: EOM schematics.

8.4 Vacuum feedthrough pins

Vacuum feedthrough is a 9-pin D-sub connector. Elements for temperature stabilization are connected according to Table 8.1 .
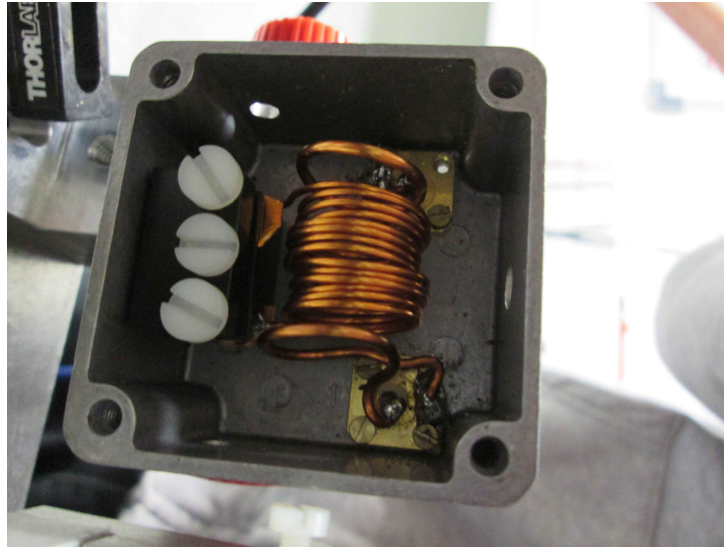
Figure 8.4: EOM image. The crystal is placed with the electrodes inside the plastic housing and tighten with the plastic screws.
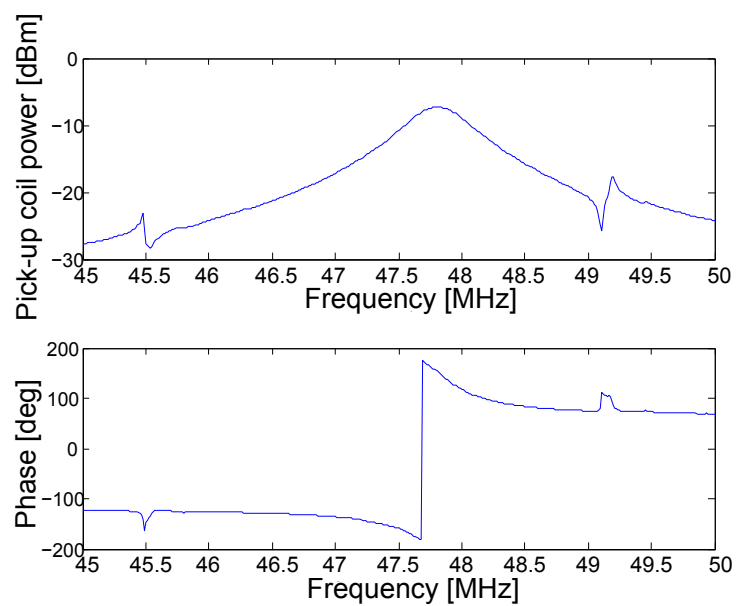

Figure 8.5: Transfer function of the self-built EOM. There are some distortions around 1 MHz away from resonance. Since EOM is used in narrower region around resonance, so this distortions should not influence its operation.

Element	Pin numbers
Peltier	3,6
Thermistor	1,2
AD590(1)	4,5
AD590(2)	8,9

Table 8.1: Pin distribution of vacuum feedthrough. There are two AD590 temperature sensors.
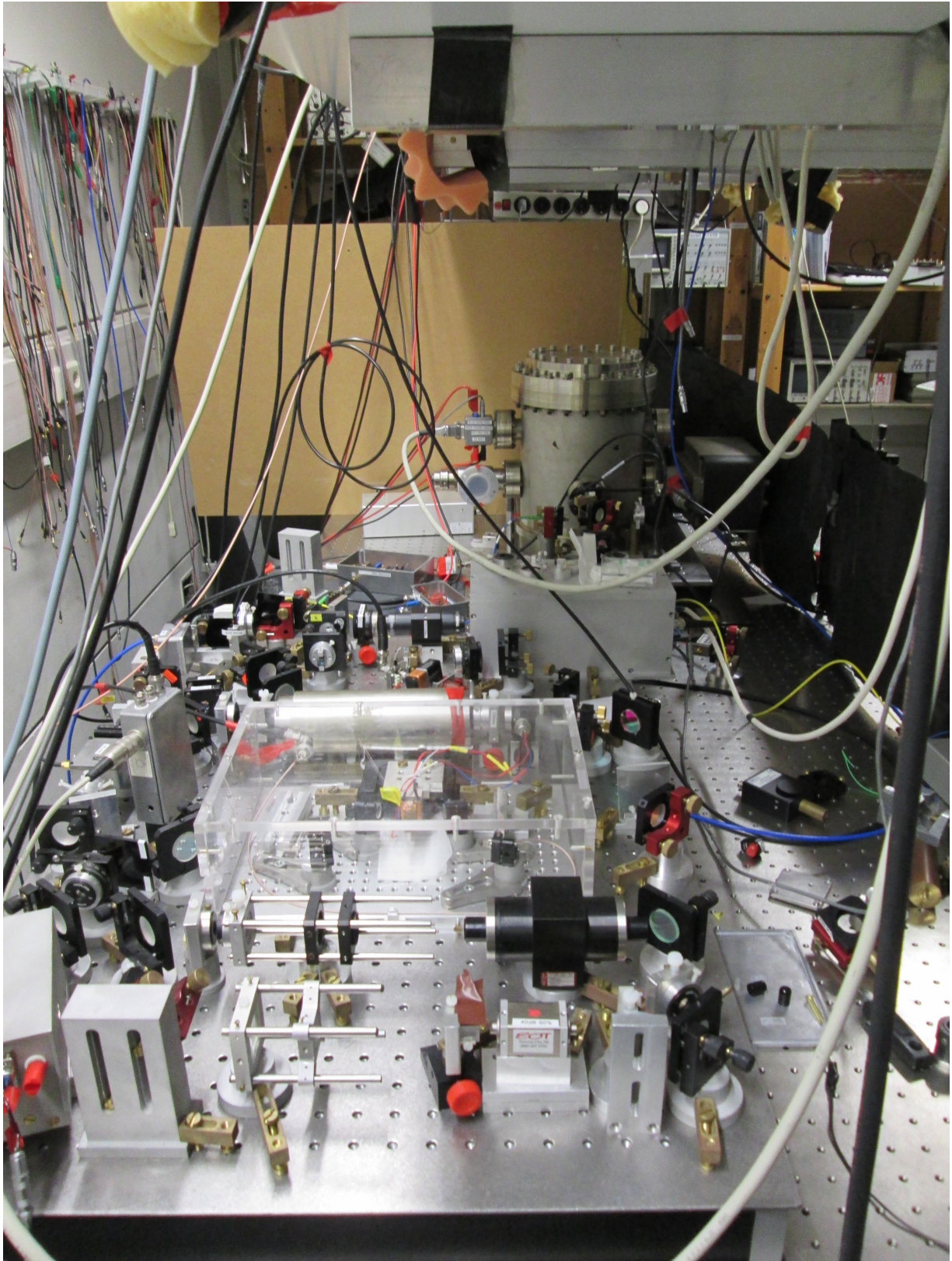
Figure 8.6: Overall setup. At the bottom left is the 960 nm diode laser. Transparent box in the middle is the housing of the doubling cavity. Behind it one can see the magnetically shielded vapor cell. Diode laser at 780nm is located behind it. In the background one can see the vacuum chamber in which the ULE cavity is placed.

Acknowledgement

Bibliography

[1] R. P. Feynman, "Simulating physics with computers," *International journal of theoretical physics*, vol. 21, no. 6, pp. 467–488, 1982.

[2] P. W. Shor, "Polynomial-time algorithms for prime factorization and discrete logarithms on a quantum computer," *SIAM journal on computing*, vol. 26, no. 5, pp. 1484–1509, 1997.

[3] D. Deutsch and R. Jozsa, "Rapid solution of problems by quantum computation," *Proceedings of the Royal Society of London. Series A: Mathematical and Physical Sciences*, vol. 439, no. 1907, pp. 553–558, 1992.

[4] J. I. Cirac and P. Zoller, "Quantum computations with cold trapped ions," *Physical review letters*, vol. 74, no. 20, p. 4091, 1995.

[5] D. Jaksch, H.-J. Briegel, J. Cirac, C. Gardiner, and P. Zoller, "Entanglement of atoms via cold controlled collisions," *Physical Review Letters*, vol. 82, no. 9, p. 1975, 1999.

[6] Y. Nakamura, Y. A. Pashkin, and J. Tsai, "Coherent control of macroscopic quantum states in a single-cooper-pair box," *Nature*, vol. 398, no. 6730, pp. 786–788, 1999.

[7] D. Loss and D. P. DiVincenzo, "Quantum computation with quantum dots," *Physical Review A*, vol. 57, no. 1, p. 120, 1998.

[8] D. P. DiVincenzo *et al.*, "The physical implementation of quantum computation," *arXiv preprint quant-ph/0002077*, 2000.

[9] G. K. Brennen, C. M. Caves, P. S. Jessen, and I. H. Deutsch, "Quantum logic gates in optical lattices," *Physical Review Letters*, vol. 82, no. 5, p. 1060, 1999.

[10] T. Pellizzari, S. Gardiner, J. Cirac, and P. Zoller, "Decoherence, continuous observation, and quantum computing: A cavity qed model," *Physical Review Letters*, vol. 75, no. 21, p. 3788, 1995.

[11] M. Saffman, T. Walker, and K. Mølmer, "Quantum information with rydberg atoms," *Reviews of Modern Physics*, vol. 82, no. 3, p. 2313, 2010.

[12] Y. Dudin and A. Kuzmich, "Strongly interacting rydberg excitations of a cold atomic gas," *Science*, vol. 336, no. 6083, pp. 887–889, 2012.

[13] D. Jaksch, J. Cirac, P. Zoller, S. Rolston, R. Côté, and M. Lukin, "Fast quantum gates for neutral atoms," *Physical Review Letters*, vol. 85, no. 10, p. 2208, 2000.

[14] T. Johnson, E. Urban, T. Henage, L. Isenhower, D. Yavuz, T. Walker, and M. Saffman, "Rabi oscillations between ground and rydberg states with dipole-dipole atomic interactions," *Physical review letters*, vol. 100, no. 11, p. 113003, 2008.

[15] L. Isenhower, E. Urban, X. L. Zhang, A. T. Gill, T. Henage, T. A. Johnson, T. G. Walker, and M. Saffman, "Demonstration of a neutral atom controlled-not quantum gate," *Phys. Rev. Lett.*, vol. 104, p. 010503, Jan 2010.

[16] D. Paredes-Barato and C. Adams, "All-optical quantum information processing using rydberg gates," *Physical review letters*, vol. 112, no. 4, p. 040501, 2014.

[17] L. Li, Y. Dudin, and A. Kuzmich, "Entanglement between light and an optical atomic excitation," *Nature*, vol. 498, no. 7455, pp. 466–469, 2013.

[18] C. Guerlin, E. Brion, T. Esslinger, and K. Mølmer, "Cavity quantum electrodynamics with a rydberg-blocked atomic ensemble," *Physical Review A*, vol. 82, no. 5, p. 053832, 2010.

[19] R. Löw, H. Weimer, J. Nipper, J. B. Balewski, B. Butscher, H. P. Büchler, and T. Pfau, "An experimental and theoretical guide to strongly interacting rydberg gases," *Journal of Physics B: Atomic, Molecular and Optical Physics*, vol. 45, no. 11, p. 113001, 2012.

[20] K. J. Weatherill and C. S. Adams, "Nonlinear optics using cold rydberg atoms," *Annual review of cold atoms and molecules*, vol. 1, p. 301, 2012.

[21] R. Heidemann, U. Raitzsch, V. Bendkowsky, B. Butscher, R. Löw, L. Santos, and T. Pfau, "Evidence for coherent collective rydberg excitation in the strong blockade regime," *Physical review letters*, vol. 99, no. 16, p. 163601, 2007.

[22] S. E. Anderson, K. Younge, and G. Raithel, "Trapping rydberg atoms in an optical lattice," *Physical review letters*, vol. 107, no. 26, p. 263001, 2011.

[23] B. Huber, T. Baluktsian, M. Schlagmüller, A. Kölle, H. Kübler, R. Löw, and T. Pfau, "Ghz rabi flopping to rydberg states in hot atomic vapor cells," *Physical review letters*, vol. 107, no. 24, p. 243001, 2011.

[24] W. Demtröder, *Laser spectroscopy*. Springer, 1982, vol. 3.

[25] R. Reimann, "Cooling and cooperative coupling of single atoms in an optical cavity," Ph.D. dissertation, University of Bonn, 2014.

[26] A. Yariv and P. Yeh, *Photonics: Optical Electronics in Modern Communications (The Oxford Series in Electrical and Computer Engineering)*. Oxford University Press, Inc., 2006.

[27] W. Treppe, "Ein stabiler resonator fur eine diodelaserstabilisierung," Master's thesis, University of Bonn, 1995.

[28] S. Linden, "Lecture notes on photonic devices."

[29] T. Nazarova, "Towards the quantum noise limit in ramsey-bordé atom interferometry," Ph.D. dissertation, 2007.

[30] T. Legero, T. Kessler, and U. Sterr, "Tuning the thermal expansion properties of optical reference cavities with fused silica mirrors," *JOSA B*, vol. 27, no. 5, pp. 914–919, 2010.

[31] R. Drever, J. L. Hall, F. Kowalski, J. Hough, G. Ford, A. Munley, and H. Ward, "Laser phase and frequency stabilization using an optical resonator," *Applied Physics B*, vol. 31, no. 2, pp. 97–105, 1983.

[32] K. Schröner, "Ein phasenstabilisiertes lasersystem für resonatorinduzierte raman-prozesse," Master's thesis, University of Bonn, 2008.

[33] T. Okoshi, K. Kikuchi, and A. Nakayama, "Novel method for high resolution measurement of laser output spectrum," *Electronics letters*, vol. 16, no. 16, pp. 630–631, 1980.

[34] W. P. Risk, T. R. Gosnell, and A. V. Nurmikko, *Compact blue-green lasers.* Cambridge University Press, 2003.

[35] G. Boyd and D. Kleinman, "Parametric interaction of focused gaussian light beams," *Journal of Applied Physics*, vol. 39, no. 8, pp. 3597–3639, 1968.

[36] J.-I. Kim, "Efficient sub-doppler transverse laser cooling of an indium atomic beam," Ph.D. dissertation, University of Bonn, 2009.

[37] T. Hansch and B. Couillaud, "Laser frequency stabilization by polarization spectroscopy of a reflecting reference cavity," *Optics communications*, vol. 35, no. 3, pp. 441–444, 1980.

[38] R. Abel, A. Mohapatra, M. G. Bason, J. Pritchard, K. Weatherill, U. Raitzsch, and C. Adams, "Laser frequency stabilization to excited state transitions using electromagnetically induced transparency in a cascade system," *Applied Physics Letters*, vol. 94, no. 7, p. 071107, 2009.

[39] A. Kasapi, M. Jain, G. Yin, and S. E. Harris, "Electromagnetically induced transparency: propagation dynamics," *Physical review letters*, vol. 74, no. 13, p. 2447, 1995.

[40] T. Peyronel, O. Firstenberg, Q.-Y. Liang, S. Hofferberth, A. V. Gorshkov, T. Pohl, M. D. Lukin, and V. Vuletić, "Quantum nonlinear optics with single photons enabled by strongly interacting atoms," *Nature*, vol. 488, no. 7409, pp. 57–60, 2012.

[41] A. Mohapatra, T. Jackson, and C. Adams, "Coherent optical detection of highly excited rydberg states using electromagnetically induced transparency," *Physical review letters*, vol. 98, no. 11, p. 113003, 2007.

[42] M. Fleischhauer, A. Imamoglu, and J. P. Marangos, "Electromagnetically induced transparency: Optics in coherent media," *Reviews of Modern Physics*, vol. 77, no. 2, p. 633, 2005.

[43] M. O. Scully, *Quantum optics*. Cambridge university press, 1997.

[44] J. Gea-Banacloche, Y.-q. Li, S.-z. Jin, and M. Xiao, "Electromagnetically induced transparency in ladder-type inhomogeneously broadened media: Theory and experiment," *Physical Review A*, vol. 51, no. 1, p. 576, 1995.

[45] M. Mack, F. Karlewski, H. Hattermann, S. Höckh, F. Jessen, D. Cano, and J. Fortágh, "Measurement of absolute transition frequencies of rb 87 to ns and nd rydberg states by means of electromagnetically induced transparency," *Physical Review A*, vol. 83, no. 5, p. 052515, 2011.

[46] E. D. Black, "An introduction to pound–drever–hall laser frequency stabilization," *American Journal of Physics*, vol. 69, no. 1, pp. 79–87, 2001.

I hereby certify that the work presented here was accomplished by myself and without the use of illegitimate means or support, and that no sources and tools were used other than those cited.

Bonn, October 14th 2014   Igor Marinković